Chapter 3
Solar-Pumped Solid-State Laser Theory

Dawei Liang [ORCID]

3.1 Brief Introduction

Properties of laser radiation and photons are firstly introduced. To comprehend solar irradiance and solar-pumped solid-state laser theory, Planck's law, Stefan-Boltzmann's law and Wien's law are presented and reinforced by several homework with solutions. The concept of spontaneous emission, stimulated absorption, stimulated emission, Einstein coefficients and thermodynamic treatment are then explained, leading to the definition of important parameters such as photon degeneracy, laser gain and stimulated emission cross section. Upper level laser rate equation, light increment along an active medium and laser oscillation threshold condition are consequently defined. More importantly, laser rate equation involving a laser resonant cavity is presented, permitting laser photon density calculation within the resonant cavity. To calculate solar laser output power, important definitions like solar concentration ratio, transfer efficiency, absorption efficiency, upper state efficiency, beam overlap efficiency and output coupling efficiency are explained. With the help of Zemax® software, the deviation angles and the effective absorption length of a solar pump ray within a laser rod are determined. A simplified Nd:YAG absorption spectrum is also provided, facilitating considerably the calculation of absorbed solar power density and absorbed pump photon number density within five simplified absorption bands of the Nd:YAG medium. Consequently, a modified analytical method for solar laser power calculation is put forward. Solar laser power from both a side-pumped laser and an end-side-pumped laser are finally calculated by the modified, classical, Zemax® and LASCAD™ analysis methods. In this chapter, we shall outline the basic theory underlying the operation of solar-pumped solid-state lasers. In-depth treatments of laser physics can be found in a number of excellent textbooks [1–6].

3.2 Properties of Laser Radiation

Laser radiation is characterized by an extremely high degree of directionality, monochromaticity, coherence, and brightness.

3.2.1 Directionality

Laser emits a well-defined beam in a specific direction, which implies laser light is of very small divergence. This is a direct consequence of the fact that a laser beam comes from a resonant cavity, and only waves propagating along the optical axis can be sustained in the cavity. The direction of the beam is governed by the orientation of the mirrors in the cavity. The directionality is described by the light beam divergence angle. For perfect spatial coherent light, a beam of aperture diameter D will have unavoidable divergence because of diffraction. From diffraction theory, the divergence angle θ_d is given by

$$\theta_d = \frac{\beta\lambda}{D} \tag{3.1}$$

where λ and D are the wavelength and the diameter of the beam respectively. β is a coefficient whose value is around unity and depends on the type of light amplitude distribution and the definition of beam diameter. θ_d is defined as diffraction limited divergence.

For a Nd:YAG laser beam with: $\lambda = 1.06\,\mu m$, $D = 3$ mm, $\beta = 1.1$, $\theta_d = \frac{\beta\lambda}{D} = 0.02227°$.

Therefore, a laser beam provides a **Very Low Beam Divergence**.

Consequently, a laser beam ensures **a Very High Focusability**.

A fundamental mode laser beam can be focused to a diffraction-limited spot size [7] (Fig. 3.1).

$$w_f = \frac{\lambda f}{\pi w_0} = \frac{630 \text{ nm} \times 10 \text{ mm}}{3.14 \times 1 \text{ mm}} = 2\,\mu m \tag{3.2}$$
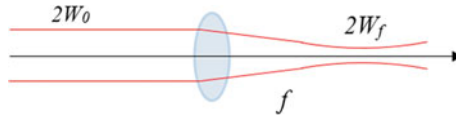

Fig. 3.1 A collimated 630 nm laser beam with $2w_0 = 2$ mm beam waist can be focused into a light spot with only $2w_f = 4\,\mu m$ beam waist

According to (3.2), for a collimated beam, the diffraction-limited focal spot size $2w_f$ of a laser beam depends on its wavelength λ, the size of the parallel beam $2w_0$ at the focusing lens and the focal length f of that lens.

3.2.2 Monochromaticity

Monochromaticity refers to a pure spectral color of a single wavelength. A laser cavity forms a resonant system. The photons are emitted by the stimulated emission where all the photons are in the same phase and in the same state of polarization. Oscillations can sustain only at the resonance frequency of the cavity. This leads to the narrowing of the laser line width. So, the laser light is usually very pure in wavelength, and the laser is therefore said to have the property of monochromaticity. In situations where only a single resonator mode has sufficient laser gain to oscillate, a single longitudinal mode can be selected, obtaining single-frequency operation. For a laser beam with $\upsilon_0 = 5 \times 10^{14}$ Hz (yellow color), typical value of $\Delta\upsilon = 1$ kHz $- 1$ MHz can be achieved by a gas laser. Using additional techniques for stabilizing the frequency, the linewidth can be further reduced by a massive extent. Some laser systems serve as optical frequency standards with a linewidth below 1 Hz [8], attaining an elevated spectral purity of 10^{-15}.

$$\frac{\Delta\upsilon}{\upsilon} = 10^{-15} \tag{3.3}$$

Quality factor of monochromaticity is defined as:

$$Q_{Monocromaticity} = \frac{\upsilon}{\Delta\upsilon} \tag{3.4}$$

3.2.3 Coherence

A very important characteristic of laser light is coherence. Coherence means that light waves are in phase. Lasers have a high degree of both spatial and temporal coherence.

Spatial coherence—for light impinging on a surface, the light is coherent if the waves (or photons) at any two points selected at random on the plane maintain a constant phase difference over time.

Temporal coherence characterizes how well a wave can interfere with itself at two different times and increases as a source becomes more monochromatic (Fig. 3.2).

Fig. 3.2 Lightwave train of wavelength λ and temporal coherence Δt from a single atom and its frequency spectrum υ with $\Delta\upsilon$ linewidth
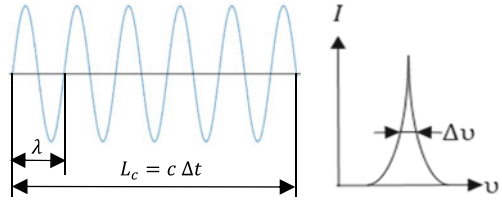
$L_c = c\,\Delta t$

Definition of coherence length

Coherence length is defined as

$$L_c = c\Delta t \tag{3.5}$$

The coherence length L_c is the coherence time Δt times the vacuum velocity of light c, and thus also characterizes the temporal coherence via the propagation length over which coherence is lost.

Since $\Delta\upsilon \simeq 1/\Delta t$, coherence length can also be presented as

$$L_c = \frac{C}{\Delta\upsilon} \tag{3.6}$$

Relations between Δt and $\Delta\upsilon$

The temporal coherence Δt comes from the monochromaticity of a laser beam. The narrower the line width $\Delta\upsilon$ of the light source, the better is its temporal coherence Δt.

$$\Delta t \simeq \frac{1}{\Delta\upsilon} \tag{3.7}$$

Relation between $\Delta\lambda$ and $\Delta\upsilon$

Since $\lambda = \frac{c}{\upsilon}$,

$$d\lambda = -\frac{c}{\upsilon^2}d\upsilon = -\frac{\lambda^2}{c}d\upsilon, \quad \text{then} \quad \frac{d\lambda}{\lambda} = -\frac{d\upsilon}{\upsilon} \tag{3.8}$$

We obtain the relationship between $\Delta\lambda$ and $\Delta\upsilon$

$$\frac{\Delta\lambda}{\lambda} = -\frac{\Delta\upsilon}{\upsilon}, \quad \left|\frac{\Delta\lambda}{\lambda}\right| = \left|-\frac{\Delta\upsilon}{\upsilon}\right| = \left|\frac{\Delta\upsilon}{\upsilon}\right| \tag{3.9}$$

Based on (3.9), the quality factor of coherence and monocromaticity is defined

$$Q_{coherence} = \frac{\lambda}{\Delta\lambda} \tag{3.10}$$

Finally, we can deduce the relations between coherence length L_c and central wavelength λ with linewidth $\Delta\lambda$.

$$L_c = c\Delta t = \frac{C}{\Delta\upsilon} = \frac{\lambda C}{\Delta\lambda\nu} = \frac{\lambda^2}{\Delta\lambda} \tag{3.11}$$

Example 1 (Homework) For a He–Ne gas laser with $\lambda = 630$ nm central wavelength and $\Delta\lambda = 0.002$ nm linewidth.

$$L_{c\ 630\ nm} = \frac{\lambda^2}{\Delta\lambda} = \frac{630^2\ nm}{0.002\ nm} = 198.45\ m,$$
$$Q_{630\ nm} = \frac{\lambda}{\Delta\lambda} = \frac{630\ nm}{0.002\ nm} = 315000$$

For a Nd:YAG solid-state laser with $\lambda = 1064$ nm central wavelength and $\Delta\lambda = 5$ nm linewidth.

$$L_{c\ 1064\ nm} = \frac{\lambda^2}{\Delta\lambda} = \frac{1064^2\ nm}{5\ nm} = 0.226\ mm,$$
$$Q_{1064\ nm} = \frac{\lambda}{\Delta\lambda} = \frac{1064\ nm}{5\ nm} = 212.8$$

Consequently, the coherence length and coherence quality factor of a He–Ne gas laser with $\lambda = 630$ nm central wavelength and $\Delta\lambda = 0.002$ nm linewidth are about 880, 1480 times higher than that of a Nd:YAG solid-sate laser with $\lambda = 1064$ nm central wavelength and $\Delta\lambda = 5.0$ nm linewidth, respectively.

3.2.4 High Brightness

While summing up the above descriptions of directionality (low divergence angle $\Delta\Omega$) and consequently focusability (small focal spot area Δs), as well as monochromaticity (narrow line width $\Delta\nu$) of a laser beam, its brightness cannot be missed out, which is defined as the power emitted per unit surface area per unit frequency and per solid angle, as indicated by (3.12). The units are watts per square meter per unit frequency and per Steradian.

$$B_\upsilon = \frac{P}{\Delta s\,\Delta\upsilon\,\Delta\Omega} \tag{3.12}$$

Laser power

Directionality

Focusability

Monochromaticity

where:

B_υ is defined as laser beam brightness.
P is the laser beam power contained within Δs, $\Delta\upsilon$ and $\Delta\Omega$.
Δs is source area, which is related to laser beam focusability.
$\Delta\upsilon$ is frequency band width, which is related to laser beam monochromaticity.
$\Delta\Omega$ is solid angle, which is related to laser beam directionality.

Since a laser beam is featured by an excellent focusablity, monochromaticity and directionality, Δs, $\Delta\upsilon$, $\Delta\Omega$ are substantially smaller than that of classical light source such as lamps, offering therefore unprecedented laser beam brightness.

TEM$_{00}$-mode laser beam brightness can also be easily defined

$$B_\upsilon = \frac{P}{A\Delta\upsilon_0\left(\pi\,\theta_0^2\right)} \tag{3.13}$$

where

B_υ represents TEM$_{00}$-mode laser beam brightness.
P denotes laser power.
A is beam cross-section area.
$\Delta\upsilon_0$ is laser linewidth.
θ_0 is beam divergence angle in the far field.

3.3 Photons

3.3.1 Concept and Properties of Photon

Photons are fundamental subatomic particles that carry the electromagnetic force. As quanta of light, photons are the smallest possible packets of electromagnetic energy. Photons are integer spin-1 ($\pm\hbar$) particles (making them bosons) and does not obey the Pauli Exclusion Principle like other half-integer spin-1/2 ($\pm\hbar/2$) fermions (electrons, protons and neutrons), but obeys the Bose–Einstein statistics.

Photons have no electric charge or rest mass. Thereore, photons are electrically neutral and are not deflected by electric and magnetic fields. Photon travels at the speed of light in empty space ($c = 2.998 \times 10^8$ m/s). However, in the presence of matter, a photon can be slowed or even absorbed, transferring energy momentum proportional to its frequency. Like all quanta, the photon has both wave and particle properties; it exhibits wave—particle duality. Today, the role of the photon as a carrier of energy is perhaps its most important attribute. The light coming from the Sun has

different wavelengths or energy and on the basis of it, we have different regions like visible, infrared, ultraviolet and many more. But one thing is common in all these regions is photon, but of different frequency and so different energy.

Photons are emitted in many natural processes, e.g., when a charge is accelerated, when an atom or a nucleus jumps from a higher to lower energy level, or when a particle and its antiparticle are annihilated (for example, electron–positron annihilation). Photons are absorbed in the time-reversed processes which correspond to those mentioned above. Photons can have particle-like interactions (i.e. collisions) with electrons and other particles, such as in the Compton Effect in which particles of light collide with atoms, causing the release of electrons.

3.3.2 Photon Energy

Each photon has a definite energy depending upon the frequency υ of the incident radiation and not on its intensity. If the intensity of light of a given wavelength is increased, there is an increase in the number of photons emitted by the incident radiations on a given area in a given time. But the energy of each photon remains unchanged.

$$E = h\upsilon = \frac{hc}{\lambda} \tag{3.14}$$

where $h = 6.626 \times 10^{-34}$ J s is Planck's constant, $c = 2.998 \times 10^8$ m/s is the speed of light and λ is the wavelength of light. All photons travel at the speed of light. The energy of a photon depends on radiation frequency; there are photons of all energies from high-energy gamma and X-rays, through visible light, to low-energy infrared and radio waves. The photon energy is inversely proportional to the wavelength of the electromagnetic wave. The shorter the wavelength, the more energetic is the photon. The longer the wavelength, the less energetic is the photon.

3.3.3 Photon Momentum

There is a relationship between photon energy E and photon momentum p and that is consistent with the relation for the relativistic total energy of a particle

$$E^2 = (pc)^2 + (mc)^2 \tag{3.15}$$

We know m is zero for a photon, but p is not, so that (3.15) becomes

$$E = p\,c \tag{3.16}$$

The momentum of a photon is related to its wavelength λ and can be calculated using the following formula

$$p = \frac{E}{c} = \frac{h\upsilon}{c} = \frac{h}{\lambda}$$ (3.17)

Photons carry linear momentum and spin angular momentum when circularly or elliptically polarized. During light—matter interaction, transfer of linear momentum leads to optical forces, whereas transfer of angular momentum induces optical torque. Optical forces including radiation pressure and gradient forces have long been used in optical tweezers and laser cooling. Space sails have been proposed that use the momentum of sunlight reflecting from gigantic low-mass sails to propel spacecraft in the solar system.

3.4 Blackbody Radiation—Planck' Law

The term blackbody comes from a theoretical model of an object absorbing all incident radiation, as shown in Fig. 3.3a that is used to develop the quantum mechanics equations. The radiated energy can be considered to be produced by standing wave or resonant modes of the cavity which is radiating. It turns out that all objects behaves like blackbodies, regardless if they are actually black or not, as shown in Fig. 3.3b.

To explain the spectral-energy distribution of radiation emitted by a blackbody, Max Planck put forward the concept of quantification of radiation energy. Energy emitted by a resonator of frequency could only take on discrete values or quanta. Planck contributed to the advancement of physics by his discovery of "Quanta".

According to Plank, for each frequency υ (each mode) → it has the energy U

$$U = \frac{h\upsilon}{e^{\frac{h\upsilon}{kT}} - 1}$$ (3.18)

For frequency interval, $\upsilon \leftrightarrow \upsilon + d\upsilon$.
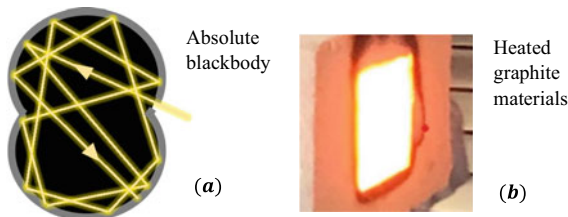

Fig. 3.3 **a** Absolute blackbody schematics. **b** Blackbody radiation from a heated graphite material

The number of radiation modes within a blackbody cavity can be calculated (See homework with solution 1)

$$n_\upsilon = \frac{8\pi \upsilon^2}{c^3} \tag{3.19}$$

Consequently, the energy density $\rho(\nu)$ in frequency interval $\upsilon \leftrightarrow \upsilon + d\upsilon$ can be calculated

$$\rho(\nu) = \frac{8\pi \upsilon^2}{c^3} U \tag{3.20}$$

When electromagnetic radiation in a cavity is in thermal equilibrium at the absolute temperature T, Planck hence formulated the theory of spectral distribution of thermal radiation

$$\rho(\upsilon) = \frac{8\pi \upsilon^2}{c^3} \frac{h\upsilon}{e^{\frac{h\upsilon}{kT}} - 1} \tag{3.21}$$

Planck's law for the energy radiated $\rho(\upsilon)$ per unit volume by a cavity of a blackbody in the frequency interval ν to $\nu + \Delta\nu$ ($\Delta\nu$ denotes an increment of frequency) can be written in terms of Planck's constant ($h = 6.626 \times 10^{-34}$ J s), the speed of light $(C = 2.998 \times 10^8$ m s$^{-1})$, the Boltzmann constant $(\kappa = 1.3806 \times 10^{-23}$ J k$^{-1})$, and the absolute temperature (T).

3.5 Solar Spectral Irradiance from Planck's Formula

In experimental work, blackbody radiation distribution according to wavelength is much more preferred.

We can deduce the spectral density $\rho(\lambda)$ in (3.22) from $\rho(\upsilon)$ in (3.21). (See homework with solution 2).

$$\rho(\lambda) = \frac{2hc}{\lambda^5} \frac{1}{e^{\frac{hc}{\lambda kT}} - 1} \tag{3.22}$$

Solar spectral irradiance $I(\lambda)$ in W m^{-2}nm^{-1} can be obtained by multiplying spectral energy density $\rho(\lambda)$ by light velocity c.

$$I(\lambda) = \rho(\lambda)\,c \tag{3.23}$$

$$I(\lambda) = \frac{2hc^2}{\lambda^5} \frac{1}{e^{\frac{hc}{\lambda kT}} - 1} \tag{3.24}$$
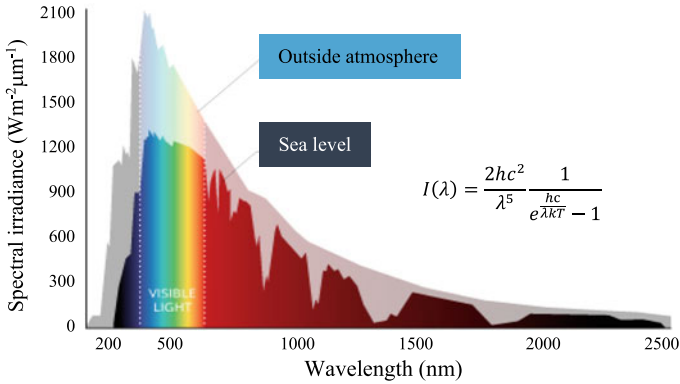
Fig. 3.4 Solar spectral irradiance at sea level and in outside atmospheric for wavelengths ranging from 240 nm to 2.5 μm. $I(\lambda) = \frac{2hc^2}{\lambda^5} \frac{1}{e^{\frac{hc}{\lambda kT}} - 1}$ can be used to approximate the solar spectral radiance curve

Equation (3.24) denotes the power emitted at a given wavelength per unit solid angle (one Steradian), per unit area (Fig. 3.4).

3.6   Stefan-Boltzmann's Law

The total radiant flux I, in unit $[\mathrm{W\,m^{-2}} = \mathrm{J\,m^{-2}s^{-1}}]$, emitted from the surface of a black body at temperature T is expressed by the Stefan-Boltzmann law:

$$I = \frac{P}{A} = \varepsilon\,\sigma\,T^4 \tag{3.25}$$

where σ denotes a fundamental physical constant called the Stefan-Boltzmann constant, σ equals to 5.67×10^{-8} w/m^{2}K^4. ε is the emissivity of the blackbody ($\varepsilon \leq 1$).

Total radiation energy density can be obtained by integrating the energy density $\rho(\nu, T)$ over all wavelengths λ. (See homework with solution 3).

Stefan-Boltzmann's law gives the radiant intensity of a single object. By Stefan-Boltzmann's law, we can also determine the radiation heat transfer between two objects. Two bodies that radiate toward each other have a net radiant power between them, as given by (3.26).

$$P_{1-2} = \varepsilon\,\sigma\,A_{1-2}\left(T_1^4 - T_2^4\right) \tag{3.26}$$

The area factor $A_{1\text{-}2}$ is the area viewed by body 2 of body 1. In many cases, body 1 can be surrounded by body 2, as shown by Fig. 3.5.

Fig. 3.5 Thermal energy transfer from body 1 to body 2, which surrounds body 1

Body 1 surrounded by body 2
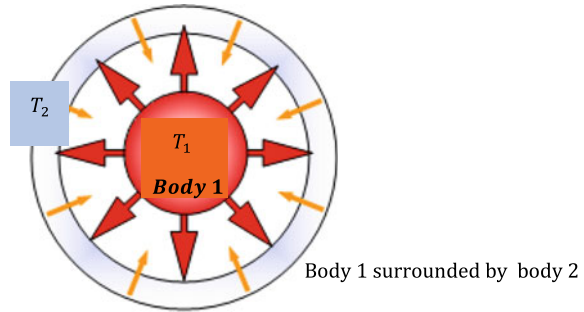
3.7 Wien's Displacement Law

Wien's displacement law is a law of physics that states that there is an inverse relationship between the wavelength of the peak of the emission of a black body and its temperature. The spectral radiance of black body radiation per unit wavelength $\rho(\lambda, T)$ peaks at the wavelength $\lambda_{\max}$, as given by (3.27)

$$\lambda_{\max} = \frac{b}{T} = \frac{2.898 \times 10^{-3} \text{ m K}}{T} \tag{3.27}$$

where T is the absolute temperature in Kelvins, b is a constant of proportionality, known as Wien's displacement constant, which equals to 2.898×10^{-3} m K.

By taking derivative of Eq. (3.24) versus wavelength λ, the peak $\rho(\lambda)$ of blackbody distribution curve can be found at $\lambda_{\max}$ (See homework with solution 4).

Example 2 (Homework)

Calculation of different peak wavelengths for different blackbody temperatures by (3.27).

Human body: $T = 310$ K $\rightarrow$ Answer ($\pmb{\lambda_{\max}} = 9.35\ \mu$m).

Molten iron: $T = 1810$ K $\rightarrow$ Answer ($\pmb{\lambda_{\max}} = 1.60\ \mu$m).

The Sun: $T = 5800$ K $\rightarrow$ Answer ($\pmb{\lambda_{\max}} = 500$ nm).

3.8 Spontaneous Emission, Stimulated Absorption and Simulated Emission Probabilities

In the early twentieth century, Max Planck formulated the theory of spectral distribution of thermal radiation. Albert Einstein, by combining Planck's theory and the Boltzmann statistics gave a theory of stimulated emission which is the governing principle of lasers. Let us assume that the material is placed in a blackbody cavity

Fig. 3.6 Simplified
2-energy level diagram
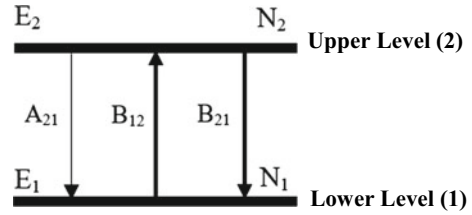
whose walls are kept at a constant temperature T. Once thermodynamic equilibrium is reached, energy density with a spectral distribution $\rho(\upsilon)$ will be established and the material will be immersed in this radiation. In this material, both stimulated-emission and absorption processes will occur, in addition to the spontaneous-emission process. There are three ways in which an incident radiation can interact with the energy levels of atoms.

To describe the phenomenon of spontaneous emission, stimulated absorption and radiations, let us consider two energy levels, lower level 1 and upper level 2, of some atom or molecule of a given material, their energies being E_1 and E_2 ($E_1 <$ E_2) (Fig. 3.6). It is important to note that the two levels could be any two out of the infinite set of levels possessed by the atom.

3.8.1 Spontaneous Emission Probability

Atoms which are in excited states are not in thermal equilibrium with their surroundings. Such atoms will eventually return to their ground state by emission of a photon. The population of the upper level will decrease due to spontaneous transition to the lower level with emission of radiation. The rate of emission will depend on the population of the upper level. Spontaneous emission is a statistical function of space and time. With a large number of spontaneously emitting atoms, there is no phase relationship between the individual emission processes; the quanta emitted are incoherent. Spontaneous emission probability A_{21} is only related to the properties of the atom itself and does not depend on with the radiation field $\rho(\upsilon)$ (Fig. 3.7).

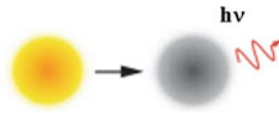Definition of spontaneous emission probability A_{21}

Fig. 3.7 Spontaneous emission: an excited atom from level (2) (lighter) transits to level (1) (darker) by releasing a photon (wiggly line)

$$A_{21} = \left(\frac{dn_{21}}{dt}\right)_{sp} \frac{1}{n_2} \tag{3.28}$$

Equation (3.28) has a solution:

$$n_2(t) = n_{20}e^{-A_{21}t} = n_{20}e^{-\frac{t}{\tau_s}} \tag{3.29}$$

where τ_s is the lifetime for spontaneous radiation of level 2. This radiation lifetime is equal to the reciprocal of the Einstein's coefficient.

$$A_{21} = \frac{1}{\tau_s} \tag{3.30}$$

Unit $A\left[\frac{1}{s}\right] = \frac{1}{230\ \mu s}$ for Nd:YAG medium.

3.8.2 Stimulated Absorption Probability

In the presence of an electromagnetic field, an atom in a lower level can undergo transitions to the upper level provided that the frequency of the radiation field $\rho(\upsilon)$ satisfies (3.31), (Fig. 3.8).

$$E_2 - E_1 = h\nu \tag{3.31}$$

However, this process is not a spontaneous one, because the atom is "stimulated to absorb" by the incident light field $\rho(\upsilon)$, W_{12} is the stimulated absorption probability of radiation, as defined below

$$W_{12} = \left(\frac{dn_{12}}{dt}\right)_{st} \frac{1}{n_1} \tag{3.32}$$

Unit $W_{12}\left[\frac{1}{s}\right]$.
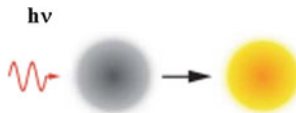
$$W_{12} = B_{12}\rho(\upsilon) \tag{3.33}$$

Fig. 3.8 Stimulated absorption: by absorption of a photon (wiggly line), the atom in the lower energy level (1) (darker) is excited to the upper level (2) (lighter)

Dimensional analysis $W_{12}\left[\frac{1}{s}\right] = B_{12}\rho(\upsilon)\left[\frac{m^3}{J\cdot s^2}\right]\left[\frac{J\cdot s}{m^3}\right]$.

Absorption pump probability W_{12} is related not only to Einstein absorption constant B_{12} but energy density of radiation $\rho(\upsilon)$ as well.

3.8.3 Stimulated Emission Probability

In 1917, Einstein showed that under certain conditions, emission of light may be stimulated by radiation incident on an excited atom. This happens when an electron is in an excited state and a photon whose energy is equal to the difference between and the energy of upper and lower energy levels. The incident photon induces the electron in the excited state to make a transition to the lower level by emission of a photon. The emitted photon travels in the same direction as the incident photon. Significantly, the new photon has the same energy as that of the incident photon and is perfectly in phase with it. When a sizable population of electrons resides in upper levels, this condition is called a "population inversion", and it sets the stage for stimulated emission of multiple photons. This is the precondition for the light amplification which occurs in a laser, and since the emitted photons have a definite time and phase relation to each other, the light has a high degree of coherence (Fig. 3.9).

W_{21} is the stimulated emission probability, as defined below:

$$W_{21} = \left(\frac{dn_{21}}{dt}\right)_{st}\frac{1}{n_2} \tag{3.34}$$

Unit $W_{21}\left[\frac{1}{s}\right]$.

$$W_{21} = B_{21}\rho(\upsilon) \tag{3.35}$$

Dimensional analysis $W_{21}\left[\frac{1}{s}\right] = B_{21}\rho(\upsilon)\left[\frac{m^3}{J\cdot s^2}\right]\left[\frac{J\cdot s}{m^3}\right]$.

Stimulated emission probability W_{12} is related not only to Einstein emission constant B_{21} but energy density of radiation $\rho(\upsilon)$ as well.
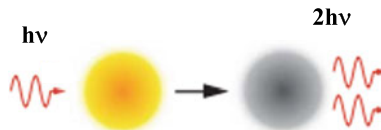

Fig. 3.9 Stimulated emission: an incident photon stimulates the excited atom to transit to lower level (1) by emitting a second photon which has the same frequency, polarization, and direction as the incident one

3.9   Einstein's Relations

Although Einstein coefficients A_{21}, B_{12}, and B_{21} are associated to different transition processes, they are all directly related to each other. If we know one of them, we can work out the rest.

Laser rate equation of upper level

$$\frac{dN_2}{dt} = \rho(\upsilon)B_{12}N_1 - \rho(\upsilon)B_{21}N_2 - A_{21}N_2 \tag{3.36}$$

Under steady state of transition

$$\frac{dN_2}{dt} = 0, \ \rho(\upsilon)B_{12}N_1 - \rho(\upsilon)B_{21}N_2 = A_{21}N_2 \tag{3.37}$$

Therefore

$$\rho(\upsilon) = \frac{A_{21}N_2}{B_{12}N_1 - B_{21}N_2} = \frac{\frac{A_{21}}{B_{21}}}{\frac{N_1}{N_2}\frac{B_{12}}{B_{21}} - 1} \tag{3.38}$$

From Boltzmann equation

$$\frac{N_1}{N_2} = e^{-\left(\frac{E_1 - E_2}{kT}\right)} = e^{\left(\frac{E_2 - E_1}{kT}\right)} = e^{\frac{h\upsilon}{kT}} \tag{3.39}$$

By inserting (3.39) into (3.38)

$$\rho(\upsilon) = \frac{\frac{A_{21}}{B_{21}}}{\frac{B_{12}}{B_{21}} e^{\frac{h\upsilon}{kT}} - 1} \tag{3.40}$$

By comparing (3.40) with Planck's formula (3.21),

$$\rho(\upsilon) = \frac{8\pi h \upsilon^3}{c^3} \frac{1}{e^{\frac{h\upsilon}{kT}} - 1} \tag{3.21}$$

We can finally find the relations of Einstein coefficients A_{21}, B_{12}, and B_{21}.

$$\frac{B_{12}}{B_{21}} = 1 \tag{3.41}$$

$$\frac{A_{21}}{B_{21}} = \frac{8\pi h \upsilon^3}{c^3} = \frac{8\pi h}{\lambda^3} \tag{3.42}$$

3.10   Photon Degeneracy in Light from Laser

From Planck's blackbody formula

$$\rho(\upsilon) = \frac{8\pi h \upsilon^3}{c^3} \frac{1}{e^{\frac{h\upsilon}{kT}} - 1} \tag{3.21}$$

We obtain

$$\frac{\rho(\upsilon)}{\frac{8\pi h \upsilon^3}{c^3}} = \frac{1}{e^{\frac{h\upsilon}{kT}} - 1} \tag{3.43}$$

From Einstein relation

$$\frac{A_{21}}{B_{21}} = \frac{8\pi h \upsilon^3}{c^3} \tag{3.42}$$

We obtain

$$\frac{\rho(\upsilon)}{\frac{8\pi h \upsilon^3}{c^3}} = \frac{\rho(\upsilon)}{\frac{A_{21}}{B_{21}}} = \frac{B_{21}\rho(\upsilon)}{A_{21}} = \frac{W_{21}}{A_{21}} = \frac{1}{e^{\frac{h\upsilon}{kT}} - 1} \tag{3.44}$$

Photon degeneracy $\bar{n}$ is finally deduced [9]

$$\bar{n} = \frac{W_{21}}{A_{21}} = \frac{1}{e^{\frac{h\upsilon}{kT}} - 1} \tag{3.45}$$

where

$W_{21} = \frac{\left(\frac{dn_{21}}{dt}\right)_{st}}{n_2} = B_{21}\rho(\upsilon)$ denotes stimulated emission probability (3.34).

$A_{21} = \frac{\left(\frac{dn_{21}}{dt}\right)_{st}}{n_2}$ denotes spontaneous emission probability (3.28).

To attain laser radiation, stimulated emisssion probability should be higher than spontaneous emission probability $W_{21} > A_{21}$, or photon degeneracy should be more than unity, $\bar{n} \geq 1$.

Example 3 (Homework)

Calculation of photon degeneracy for $\lambda = 0.6$ μm visible lightwave at different temperatures by

$$\bar{n} = \frac{W_{21}}{A_{21}} = \frac{1}{e^{\frac{h\upsilon}{kT}} - 1} \tag{3.45}$$

1. $T = 300$ K, $\lambda = 0.6$ μm
   (Answer $\bar{n} = 10^{-35}$), not possible for laser emission.

2. $T = 5000\ K$, $\lambda = 0.6\ \mu m$
   (Answer $\bar{n} = 0.08$), not possible for laser emission.
3. $T = 50000\ K$, $\lambda = 0.6\ \mu m$
   (Answer $\bar{n} = 1.54$), possible for laser emission.

Example 4 (Homework)

Calculation of photon degeneracy for $\lambda = 30$ cm microwave radiation at $T = 300\ K$.
   Answer:

$$\upsilon = \frac{c}{\lambda} = \frac{30 \times 10^9 \frac{cm}{s}}{30\ cm} = 1\ \text{GHz},$$

$$\bar{n} = \frac{1}{e^{\frac{h\upsilon}{kT}} - 1} = \frac{1}{e^{\frac{6.63 \times 10^{-34}\ \text{J·s} \times 10^9\ \text{s}^{-1}}{1.38 \times 10^{-23}\ \frac{J}{K} \times 300\ K}} - 1} = \frac{1}{e^{0.00016} - 1} = 6250 \gg 1$$

Conclusion

As shown by example 3, stimulated emission process may be significant for optical frequencies, but this requires extremely high temperature ($T = 50000$ K) to attain the minimum laser emission condition.

   $W_{21} > A_{21}$, or photon degeneracy should be more than one, $\bar{n} \geq 1$.

   For microwave frequencies, however, the stimulated emission processes can be significant even at room temperature ($T = 300$ K), as calculated by example 4. This explains why Microwave Amplification by Stimulated Emission of Radiation "MASER" was more early and easily attained than Light Amplification by Stimulated Emission of Radiation "LASER".

3.11   Laser Gain and Stimulated Emssion Cross Section

Laser rate equation for the upper level N_2 can be presented

$$\frac{dN_2}{dt} = \rho(\upsilon)B_{12}N_1 - \rho(\upsilon)B_{21}N_2 - A_{21}N_2 \tag{3.46}$$

Atomic energy levels are not infinitely sharp, but have some width associated with them. As a result, the spectrum of transition is not shap lines but have some distribution. By considering laser line shape function $g(\upsilon)$ [1–6], change in population density by stimulated emission N_{21} and change in population density by stimulated absorption N_{12} are defined:

$$N_{21} = B_{21}\ \rho(\upsilon)\ N_2\ g(\upsilon) \tag{3.47}$$

$$N_{12} = B_{12}\rho\ (\upsilon)\ N_1\ g(\upsilon) \tag{3.48}$$

$N_{21} - N_{12}$ denotes net change in population density: N_{21}^{net}.

$$N_{21}^{net} = N_{21} - N_{12} = (N_2 - N_1)\, B_{21} g(\upsilon)\, \rho(\upsilon) \tag{3.49}$$

where

$$B_{21} = B_{12}$$

Since light energy intensity $I(\upsilon)$ with unit $\left[\frac{J}{m^2}\right]$ equals to the product of photon energy density $\rho(\upsilon)$ with unit $\left[\frac{J}{m^3 H_z}\right] = \left[\frac{J \cdot s}{m^3}\right]$ and light velocity within the laser medium $\frac{c}{n}$ with unit $\left[\frac{m}{s}\right]$.

$$I(\upsilon) = \rho(\upsilon)\,\frac{c}{n}, \tag{3.50}$$

$$\rho(\upsilon) = I(\upsilon)\,\frac{n}{c} \tag{3.51}$$

Dimensional analysis of (3.50)

$$I(\upsilon)\left[\frac{J}{m^2}\right] = \rho(\upsilon)\frac{c}{n}\ \left[\frac{J \cdot s}{m^3}\right]\left[\frac{m}{s}\right]$$

Photon energy density $\rho(\upsilon)$ in (3.49) can hence be replaced by $I(\upsilon)\frac{n}{c}$.
Relation between N_{21}^{net} and $I(\upsilon)$ is found

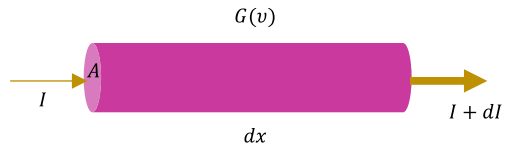$$N_{21}^{net} = (N_2 - N_1)\, B_{21}\, g(\upsilon)\,\frac{n}{c}\, I(\upsilon) \tag{3.52}$$

By adding photon energy to the active volume in Fig. 3.10.

$$N_{21}^{net}\, h\upsilon\, A\, dx \tag{3.53}$$

Light intensity increament inside the volume can be calculated:

$$dI = N_{21}^{net} h\upsilon\, dx = (N_2 - N_1)\, B_{21}\, g(\upsilon)\,\frac{n}{c} I(\upsilon)\, h\upsilon dx \tag{3.54}$$

Fig. 3.10 Light intensity I increment along an active medium with A cross-section and dx length

By considering laser gain definition

$$G(\upsilon) = \frac{\frac{dI(\upsilon)}{dx}}{I(\upsilon)} \tag{3.55}$$

$$dI = G(\upsilon)I(\upsilon)dx \tag{3.56}$$

By comparing (3.54) and (3.56), we obtain

$$G(\upsilon) = (N_2 - N_1)B_{21}g(\upsilon)\frac{n}{c}h\upsilon \tag{3.57}$$

From Einstein relation in active medium with refractive index n.

$$B_{21} = \frac{c^3}{8\pi n^3 h\upsilon^3}A_{21} \tag{3.42}$$

We finally obtain the analytical presentation of laser gain $G(\upsilon)$

$$G(\upsilon) = (N_2 - N_1)\frac{c^3 A_{21}}{8\pi n^3 h\upsilon^3}g(\upsilon)\frac{n}{c}h\upsilon = (N_2 - N_1)\frac{\lambda^2 A_{21}}{8\pi n^2}g(\upsilon) \tag{3.58}$$

A more simplified presentation of $G(\upsilon)$ is reached by using

$$A_{21} = \frac{1}{\tau_{21}} \tag{3.30}$$

$$G(\upsilon) = (N_2 - N_1)\frac{\lambda^2}{8\pi n^2 \tau_{21}}g(\upsilon) \tag{3.59}$$

One of the most important parameter of laser physics: **Stimulated Emission Cross Section** $\sigma(\upsilon)$ is finally defined as

$$\sigma(\upsilon) = \frac{\lambda^2}{8\pi n^2 \tau_{21}}g(\upsilon) \tag{3.60}$$

Sitmulated emission cross-section is purely related to the property of laser active medium, depending only on upper level lifetime τ_{21}, refractive index n, laser wavelength λ and line shape function $g(\upsilon)$ of the laser medium. Consequently, laser gain can be more simply defined as the product of the stimulated emission cross section $\sigma(\upsilon)$ and the population inversion $N_2 - N_1$.

$$G(\upsilon) = \sigma(\upsilon)(N_2 - N_1) \tag{3.61}$$

3.12   Upper Level Laser Rate Equation

In a four-level laser, a pump excites atoms, molecules, or other atomic systems from the ground state level to an excited state (pump level). A sustained laser emission can be achieved by using atoms that have two relatively stable levels between their ground level and pump level. The atoms first drop to a long-lived metastable state (Upper level N_2) where they can be stimulated to emit excess energy. However, instead of dropping to the ground level, they stop at lower level N_1 above the ground level from which they can more easily be excited back up to the higher metastable state, thereby maintaining the population inversion needed for continuous laser operation. By taking into account the contribution of pumping W_p and laser lineshape function $g(v)$, the upper level laser rate equation can be presented: (Details on how to calculate solar pump rate W_p will be explained in Sect. 3.23), (Fig. 3.11).

$$\frac{dN_2}{dt} = W_p + \rho(v)B_{12}N_1 g(v) - \rho(v)B_{21}N_2 g(v) - A_{21}N_2 \qquad (3.62)$$

From Einstein relation

$$B_{21} = B_{12} \qquad (3.41)$$

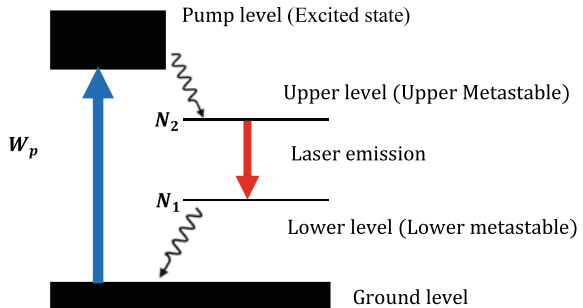$$\frac{dN_2}{dt} = W_p - \rho(v)B_{21}g(v)(N_2 - N_1) + A_{21}N_2 \qquad (3.63)$$

Since

$$\rho(v) = I(v)\frac{n}{c} \qquad (3.51)$$

$$B_{21} = A_{21}\frac{c^3}{8\pi n^3 h v^3} \qquad (3.42)$$

$$\rho(v)B_{21}g(v) = I(v)\frac{n}{c}A_{21}\frac{c^3}{8\pi n^3 h v^3}g(v) = \frac{A_{21}\lambda_0^2}{8\pi n^2}g(v)\frac{I(v)}{hv} = \sigma(v)\frac{I(v)}{hv} \qquad (3.64)$$

where $\sigma(v) = \frac{A_{21}\lambda_0^2}{8\pi n^2}g(v)$.

Fig. 3.11 Schematics of a four-level laser system. Wiggle lines indicate fast non-radiative transitions. Blue solid line for pump transition and red solid line for slow laser transition

We can finally replace $\rho(v)B_{21}g(v)$ by $\sigma(v)\frac{I(v)}{hv}$ in (3.63).

Finally, we obtain an important laser rate equation involving pump rate W_p, stimulated emission cross section $\sigma(v)$, number of photons per unit area per unit time $\frac{I(v)}{hv}$, upper level pupulation N_2, lower level population N_1 and spontaneous emission constant A_{21}.

$$\frac{dN_2}{dt} = W_p - \sigma(v)\frac{I(v)}{hv}(N_2 - N_1) + A_{21}N_2$$

(3.65)

| Pump rate | Stimulated emission cross-section | Number of photons per unit area per unit time | Stimulated emission | Absorption | Spontaneous emission |

3.13 Light Intensity Increment Along Active Medium

At steady state oscillation, the populations is independent of time

$$\frac{dN_2}{dt} = 0$$

(3.66)

Due to the rapid transition from lower level to ground level, zero population $N_1 = 0$ for the lower level is assumed.

Consequently

$$\frac{dN_2}{dt} = W_p - \sigma\frac{I}{hv}(N_2 - 0) + A_{21}N_2 = 0$$

(3.67)

Since

$$A_{21} = \frac{1}{\tau}$$

(3.30)
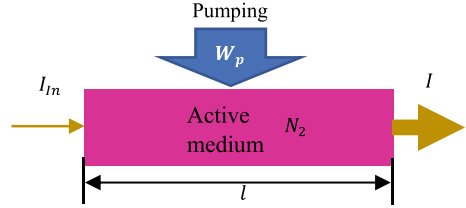
$$\frac{dN_2}{dt} = W_p - \frac{\sigma I}{hv}N_2 - \frac{N_2}{\tau} = 0$$

(3.68)

Then

$$N_2 = \frac{W_p\tau}{1 + \frac{\sigma\tau}{hv}I} = \frac{W_p\tau}{1 + \frac{I}{\frac{hv}{\sigma\tau}}} = \frac{W_p\tau}{1 + \frac{I}{I_S}}$$

(3.69)

where W_p is the pump rate in unit $\left[\frac{1}{s}\right]$.

Fig. 3.12 Laser light intensity increament along an active medium

Saturation intensity I_S is hence defined

$$I_S = \frac{h\upsilon}{\sigma\tau} \tag{3.70}$$

$$I_S = \frac{h\upsilon}{\sigma\tau} = 2.9\frac{\text{kW}}{\text{cm}^2} \text{ for Nd:YAG medium}$$

When $I = 0$, population inversion N_2 reaches its maximum value

$$N_2(0) = W_p\tau \tag{3.71}$$

Therefore, the relation between population inversion in upper level N_2 and laser light intensity I is found (Fig. 3.12).

$$N_2 = \frac{N_2(0)}{1 + \frac{I}{I_{Sat}}} \tag{3.72}$$

By laser gain definition

$$G(\upsilon) = \frac{\frac{dI(\upsilon)}{dx}}{I(\upsilon)} \tag{3.55}$$

$$dI = G(\upsilon)I(\upsilon)dx = \sigma(\upsilon)(N_2 - N_1)I(\upsilon)dx \tag{3.73}$$

By assuming zero lower level pupulation $N_1 = 0$ for (3.73) and using (3.72)

$$\frac{dI}{dx} = \sigma I(N_2 - N_1) \approx \sigma IN_2 = \sigma I\frac{N_2(0)}{1 + \frac{I}{I_{Sat}}} \tag{3.74}$$

Therefore

$$\int_{I_{in}}^{I} \frac{dI}{I} + \int_{I_{in}}^{I} \frac{dI}{I_{Sat}} = \int_{0}^{l} \sigma N_2(0)dx \tag{3.75}$$

$$ln\frac{I}{I_{in}} + \frac{I - I_{in}}{I_{Sat}} = \int_{0}^{l} \sigma N_2(0)dx \tag{3.76}$$

Equation (3.76) can be solved numerically.
Simplified solution for (3.76) can be found in two following cases

1. $I \ll I_{Sat}$ (Weak pumping), $\frac{I}{I_{Sat}}$ is negligible in (3.74)

Therefore (Fig. 3.13)

$$\frac{dI}{I} = \sigma N_2(0)dx \tag{3.77}$$

$$I(z) = e^{\sigma N_2(0)x} \tag{3.78}$$

2. $I \gg I_{Sat}$ (Very strong pumping), $\ln \frac{I}{I_{In}}$ is negligible in (3.76)

Equation (3.76) can then be simplified to (Fig. 3.14)

$$\frac{I - I_{in}}{I_{Sat}} = \int_0^l \sigma N_2(0) \, dx \tag{3.79}$$

$$I = I_{in} + I_{Sat} \int_0^l \sigma N_2(0) dx \tag{3.80}$$

Fig. 3.13 Light intensity inceases exponentially with x

$$I(z) = e^{\sigma N_2(0) x}$$
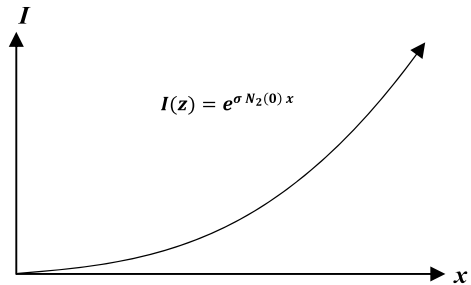
Fig. 3.14 Light intensity increases much more slowly, as compared to that of Fig. 3.13

$$I = I_{in} + I_{Sat} \int_0^l \sigma N_2(0) \, dx$$
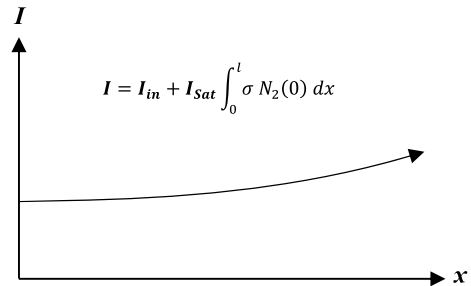
3.14   Laser Oscillation Threshold Condition

Laser intensity enhencement I' after one round-trip, starting from I at point A and ending at the same point (Fig. 3.15).

$$I' = I R_1 R_2 (1 - L_i)^2 e^{2\sigma [N_2 - N_1]l} \tag{3.81}$$

For a laser resonator composed of a HR end mirror with laser wavelength reflectance of R_1 (approaching 100%), a PR output mirror with laser wavelength reflectance of R_2 (may vary between 40 and 99% for example), an active medium with rod length l and loss L_i, laser oscillation threshold condition can be determined by assuming $I' = I$, leading to the following equation

$$R_1 R_2 (1 - L_i)^2 e^{2\sigma [N_2 - N_1]l} = 1 \tag{3.82}$$

$$e^{2\sigma [N_2 - N_1]l} = \frac{1}{R_1 R_2 (1 - L_i)^2} \tag{3.83}$$

Therefore

$$2\sigma [N_2 - N_1]l = -[\ln(R_1 R_2) + 2\ln(1 - L_i)] \tag{3.84}$$

Threshold population inversion density can be calculated

$$N_2 - N_1 = -\frac{1}{2\sigma l}[\ln(R_1 R_2) + 2\ln(1 - L_i)] \tag{3.85}$$

It is convenient to introduce some new quantities γ, which can be described as the logarithmic loss per pass, namely.

$$\gamma_1 = -\ln R_1 = -\ln(1 - T_1) \tag{3.86}$$

$$\gamma_2 = -\ln R_2 = -\ln(1 - T_2) \tag{3.87}$$

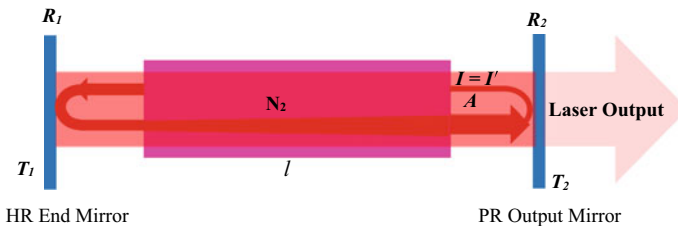$$\gamma_i = -\ln(1 - L_i) \tag{3.88}$$

Fig. 3.15 Schematics of laser intensity variation in round-trip within a laser resoant cavity
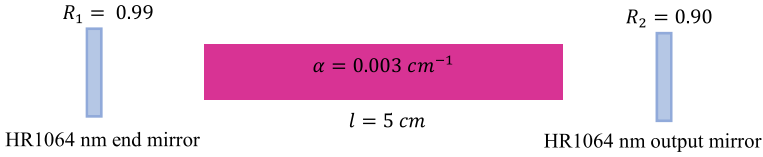
$R_1 = 0.99$

$\alpha = 0.003\ cm^{-1}$

$R_2 = 0.90$

$l = 5\ cm$

HR1064 nm end mirror

HR1064 nm output mirror

Fig. 3.16 Laser resonant cavity composed of a Nd:YAG rod, a HR1064 nm end mirror and a PR1064 nm output mirror

γ_1 and γ_2 are the logarithmic losses per pass due to the mirror transmission and γ_i is the logarithmic internal loss per pass. T_1 and T_2 are laser wavelength reflectivities of the HR end mirror and the PR output mirror, respectively. The logarithmic loss notation proves to be the most convenient way of representing laser losses, given the exponential character of the laser gain. Threshold population inversion density $N_2 - N_1$ can hence be presented.

$$N_2 - N_1 = \frac{1}{2\sigma l}\left[\gamma_1 + \gamma_2 + 2\gamma_i\right] = \frac{1}{\sigma l}\left[\gamma_i + \frac{1}{2}(\gamma_1 + \gamma_2)\right] = \frac{\gamma}{\sigma l} \qquad (3.89)$$

Example 5 Calulation of threshold population inversion density $N_2 - N_1$ for a laser resonator with a $l = 5$ cm length Nd:YAG rod with $\sigma = 3 \times 10^{-19}$ cm^2 stimulated emission cross section and $\alpha = 0.003$ cm^{-1} absorption and scattering loss coefficient.

By using laser resoant cavity parameters indicated in Fig. 3.16

$\gamma_1 = -\ln R_1 = -\ln 0.99 = 0.01,$ $\qquad\qquad$ $\gamma_2 = -\ln R_2 = -\ln 0.90 = 0.105$

$L_i = 2\alpha l = 2 \times 0.003$ cm$^{-1} \times 5$ cm $= 0.03$ $\quad \gamma_i == -\ln(1 - L_i) = \ln(1 - 0.03)$

$\qquad = 0.03$

Threshold population inversion density $N_2 - N_1$ for the Nd:YAG medium can be calculated by (3.89)

$$N_2 - N_1 = \frac{1}{2\sigma l}\left[\gamma_1 + \gamma_2 + 2\gamma_i\right]$$
$$= \frac{1}{2 \times 3 \times 10^{-19}\ \text{cm}^2 \times 5\ \text{cm}}(0.01 + 0.105 + 0.06)$$
$$= 5.83 \times 10^{16}\ \text{cm}^{-3}$$

3.15   Laser Rate Equation Involving Resonant Cavity

As shown in Fig. 3.17, by photon absorption, atoms are excited to upper laser level at a pump rate W_p per second per unit volume, the rate equations for a four-level material can be used [10]

$$\frac{dN}{dt} = W_p(N_t - N) - \rho\sigma cN - \frac{N}{\tau_e} \tag{3.90}$$

$$\frac{d\rho}{dt} = \frac{c}{L'}(\sigma lN - \gamma)\rho \tag{3.91}$$

where W_p is the pump rate, N is the population inversion density, N_t is the total number density of the active atoms in the laser rod (for 1.0 at.% $Nd^{3+}YAG$ medium, $N_t = 1.38 \times 10^{20}$ cm^{-3}), c is the velocity of light in vacuum, σ is the stimulated emission cross section, τ_e is the effective lifetime of the upper laser level, and ρ is the photon density in the laser cavity. L' is the effective cavity length and is given as

$$L' = L_C + (n - 1)l \tag{3.92}$$

where L_C is the length between the two cavity mirrors, n is the refractive index of the laser host material, and l is the length of the laser material.

For a laser resonator with an active medium, γ represents the logarithmic loss by the scattering and absorption of the laser light in the laser material and by the transmission of the two laser cavity mirrors, γ is thus given as

$$\gamma = \alpha l + \frac{1}{2}\left[\ln\left(\frac{1}{R_1}\right) + \ln\left(\frac{1}{R_2}\right)\right] \tag{3.93}$$

where α is the scattering and absorption losses per unit length, R_1 is the reflectance of the full mirror, and R_2 is the reflectance of the output coupler mirror.

The first term on the right-hand side of (3.91) represents the rate of photon density increase in the laser cavity by stimulated emission and the second term represents the
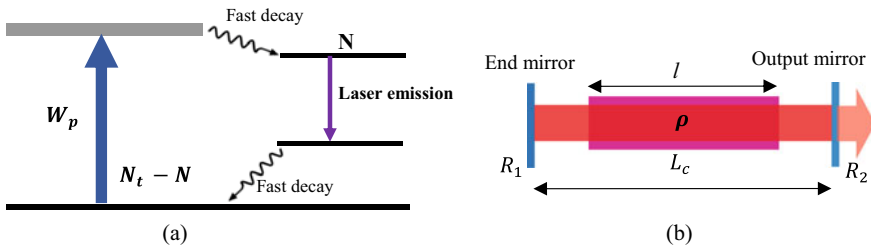

Fig. 3.17   **a** Simplified energy-level diagram of a four-level laser, **b** Schematics of a laser resonant cavity

photon loss rate due to the scattering and to the transmittance of the cavity mirrors. The photon loss rate coefficient can hence be written as

$$\frac{\gamma c}{L'} = \frac{\alpha c l}{L'} + \frac{c}{2L'}\left[\ln\left(\frac{1}{R_1}\right)\right] + \frac{c}{2L'}\left[\ln\left(\frac{1}{R_2}\right)\right]$$

(3.94)

3.16 Calculation of Photon Density Within a Laser Resonant Cavity

The population inversion in the laser cavity while the laser is in CW oscillation can be calculated from the photon rate Eq. (3.90) by applying the time invariant condition of the population density: $\frac{dN}{dt} = 0$

$$W_p N_t = \left(W_p + \rho \sigma c + \frac{l}{\tau_e}\right)N$$

(3.95)

Also, by applying the time invariant condition of the photon density $\frac{d\rho}{dt} = 0$ to (3.91) at the threshold

$$\sigma l N_c - \gamma = 0$$

(3.96)

$$N_c = \frac{\gamma}{\sigma l}$$

(3.97)

where threshold inversion population N_c is proportional to the single-trip cavity loss γ and inversely proportional to the product of the stimulated emission cross-section σ and the rod length l.

Since the population inversion density N is clamped at the threshold inversion density N_c [1]

$$N = N_c = \frac{\gamma}{\sigma l}$$

(3.98)

By applying (3.98) to (3.95)

$$W_p N_t = \left(W_p + \rho \sigma c + \frac{l}{\tau_e}\right)\frac{\gamma}{\sigma l}$$

(3.99)

The photon density ρ within the laser cavity is finally obtained.

$$\rho = \frac{1}{\sigma c}\left[\left(\frac{N_t \sigma l}{\gamma} - 1\right)W_p - \frac{1}{\tau_e}\right]$$

(3.100)

3.17   Solar Concentration Ratio

The ratio between the concentrated flux on the receiver and the ambient flux from the sun is called the optical concentration ratio. Geometric concentration ratio C is defined as the area of solar collector S_a divided by the surface area of the receiver S_r. The laser rod surface can be considered as a receiver.

$$C = \frac{S_a}{S_r} = \frac{S_a}{\pi Dl} \qquad (3.101)$$

where S_a is primary solar collector area, πDl is the laser rod side surface area exposed to concentrated solar pump rays.

3.18   Transfer Efficiency

Transfer Efficiency η_T can be defined as the ratio between the solar power incident on laser active medium and the incoming solar power reaching the primary solar collector [11].

$$\eta_T = \frac{\int_{\lambda_1}^{\lambda_2} \eta_{tg}\, \eta_{tl}(\lambda) I(\lambda) d\lambda}{\int_{\lambda_1}^{\lambda_2} I(\lambda) d\lambda} \qquad (3.102)$$

where

η_{tg} is a geometrical transfer factor from the solar collector to the surface of the laser medium and is usually independent of wavelength.

$\eta_{tl}(\lambda)$ takes into account the reflection and transmission losses of primary, secondary solar concentrators and laser pump cavity.

The absorption by cooling liquid, the reflection and scattering losses at the laser medium and flow tube should be considered.

The integral in (3.102) is taken over the wavelength range between λ_1 and λ_2, which are useful for pumping the upper laser level. As an example, solar spectral irradiance $I(\lambda)$ and complex absorption spectra $\alpha(\lambda)$ of 1.0 at. % Nd:YAG medium are presented by orange and blue lines, respectively in Fig. 3.18. The integral in (3.102) is taken over the wavelength range from $\lambda_1 = 530$ nm to $\lambda_2 = 880$ nm for pumping the upper laser level.
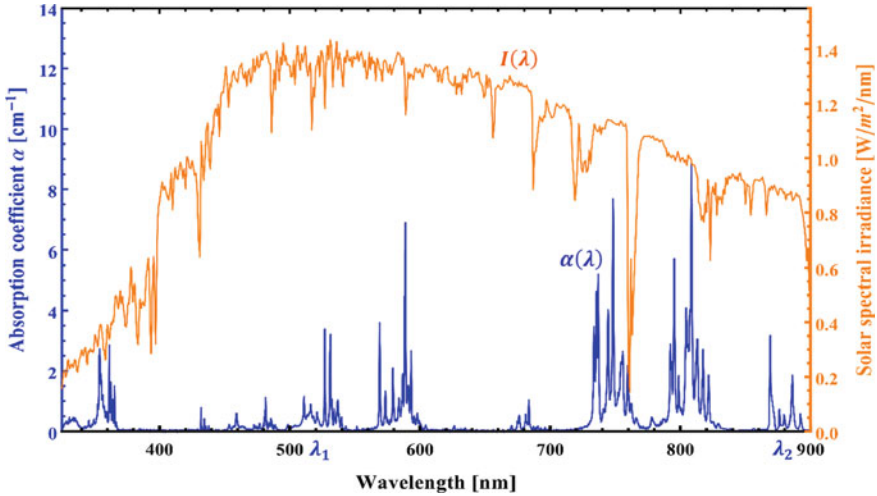
Fig. 3.18 Standard solar emission spectrum $I(\lambda)$ (orange line), Nd:YAG absorption spectrum $\alpha(\lambda)$ (blue line)

3.19   Absorption Efficiency

Absorption Efficiency η_A describes conversion of incident solar power incident on the surface of the active medium to the total absorbed pump power by the same medium.

Absorption efficiency η_A can be defined as [11]

$$\eta_A = \frac{P_a}{\int_{\lambda_1}^{\lambda_2} P_{e\lambda} d\lambda} \tag{3.103}$$

where:

P_a is the total absorbed solar power by the active medium.
$P_{e\lambda}$ is the power per unit wavelength incident on the medium.

For solar-pumped solid-state lasers, absorption efficiency calculations require the absorption spectra of the laser material and the solar emission spectra, as shown in Fig. 3.18, where pump source is characterized by solar spectral distribution $I(\lambda)$, and the laser material is characterized by absorption coefficients $\alpha(\lambda)$.

In addition, the angular distribution of the concentrated solar light on the laser material, as well as the geometry of the laser material and its refractive index also need to be known.

For solid-state lasers, the pump source is characterized by a relative spectral distribution $I(\lambda)$, and the laser material is characterized by an absorption coefficient $\alpha(\lambda)$, as shown in Fig. 3.18.

The pump photons have a distribution of incident angles $F(\theta, \varphi)$, and travel a path length $L(\theta, \varphi)$ in the laser material which depends on the incident angles θ and φ.

Given this, the absorption efficiency can be found [12]

$$\eta_A = \frac{\int_{\lambda_1}^{\lambda_2} \int_0^{\frac{\pi}{2}} \int_0^{\frac{\pi}{2}} \frac{\lambda}{\lambda_L} I(\lambda) F(\theta, \phi)\{1 - exp[-\alpha(\lambda)L]\} sin\theta d\theta d\phi d\lambda}{\int_{\lambda_1}^{\lambda_2} \int_0^{\frac{\pi}{2}} \int_0^{\frac{\pi}{2}} I(\lambda) F(\theta, \phi) d\theta d\phi d\lambda} \qquad (3.104)$$

where

Integration is over all incident angles allowed by the angular distribution $F(\theta, \phi)$.

Integration over wavelength is all wavelengths emitted by the pump source.

L is defined as the effective absorption length of pump light within the laser rod.

$\alpha(\lambda)$ is the absorption coefficient of the laser medium.

λ_L is the laser wavelength.

$1/\lambda_L$ is used to normalize so the efficiency is dimensionless.

Integration may vary between $\lambda_1 = 0.3$ µm to $\lambda_2 = 2.4$ µm for solar-pumped lasers.

However, when an active medium has a limited absorption bandwidth, integration over wavelength may vary only from $\lambda_1 = 0.5$ µm to $\lambda_2 = 0.88$ µm, as for the case of solar pumping of Nd:YAG material, as indicated in Fig. 3.18.

3.20   Deviation Angle and Effective Absorption Length

Numerically, the non-sequential method of Zemax® program can be used for calculating the above mentioned transfer efficiency η_T by (3.102) and absorption efficiency η_a by (3.103).

As shown in Fig. 3.19, a detector rectangle can be placed beneath the laser rod surface in Zemax® program. The deviation angles of α and β in transversal and longitudinal directions, respectively, can be detected by using the irradiance (angle space) function of the detector rectangle in Zemax® program [13].

Once α and β are found, the most important parameter in Fig. 3.19, defined as the deviation angle of the solar pump ray within the laser rod, β' can be calculated

$$\tan \beta' = \cos \alpha \, \tan \beta \qquad (3.105)$$

Effective absorption length L of the solar pump ray can be finally calculated

$$L = \frac{D}{\cos \alpha \cos \beta'} \qquad (3.106)$$

As compared to the complicated analytical modeling by (3.102) and (3.104), transfer efficiency η_T and absorption efficiency η_a can be more accurately and easily calculated by Zemax® software.
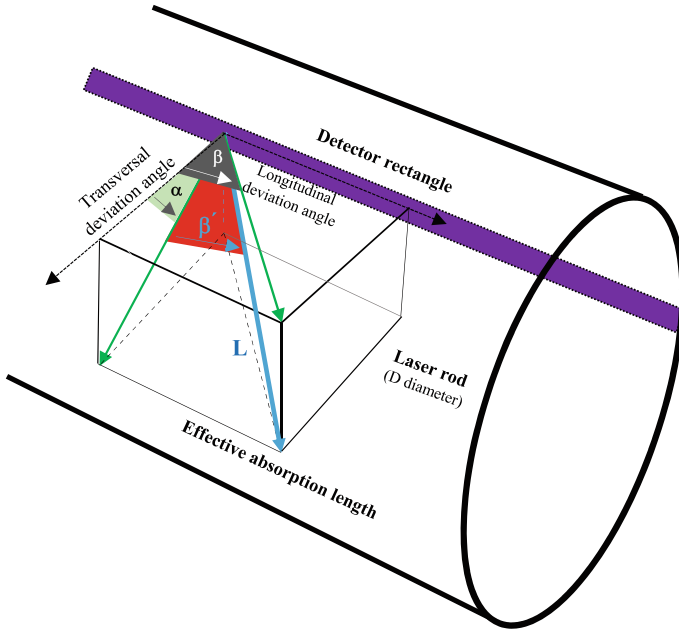
Fig. 3.19 Sun ray propagation geometry within a laser rod with D diameter. In Zemax® analysis, a rectangular detector can be positioned beneath the rod surface to detect the transversal deviation angle α and longitudinal deviation angle β of a solar pump ray within the laser rod, so as to calculate the deviation angle of solar pump ray β'. Effective absorption length L can be consequently determined

By assuming an infinite absorption coefficient $\alpha(\lambda) = \infty$ for a laser medium, all the incident rays are considered absorbed by the laser rod surface.

A rectangular volume detector can be used to calculate the total solar pump power incident on the surface of the laser rod, as shown in Fig. 3.20. Consequently, transfer efficiency can hence be calculated by (3.107).

$$\eta_T = \frac{P_{Rod\ surface}}{P_{Primar\ collector}} \qquad (3.107)$$

where

$P_{Rod\ surface}$ denotes the solar pump power incident on the surface of the laser rod, as indicated by Fig. 3.20.

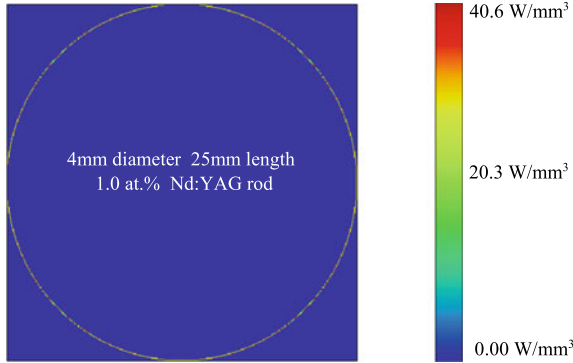$P_{Primar\ collector}$ denotes the total incoming solar power reaching the primary solar collector.

Fig. 3.20 Zemax® rectangular volume detector for the simulation of solar power reaching the surface of a Nd:YAG laser rod. Red color means near maximum solar energy absorption, whereas blue means little or no absorption. Numerical simulation data was obtained by analyzing the absorbed flux/volume profile of a 4 mm diameter, 25 mm length 1.0 at.% Nd:YAG pumped by a 0.636 m² Fresnel lens [14]

3.21 Upper State Efficiency

Upper State Efficiency $\eta_U(\lambda)$ is defined as the product of two contributing factors

1. Quantum efficiency $\eta_Q(\lambda)$.
2. Quantum defect efficiency $\eta_s(\lambda)$, also referred as Stokes factor.

$$\eta_U(\lambda) = \frac{P_U}{P_A} = \eta_Q(\lambda)\,\eta_S(\lambda) \tag{3.108}$$

Quantum Efficiency $\eta_Q(\lambda)$ can be defined as the ratio of the number of atoms raised to the upper laser level to the number of absorbed pump photons [11]. It relates the probability of an absorbed photon producing an atom in the upper laser level. We can thus write:

$$\eta_Q(\lambda) = \frac{h\upsilon \int \frac{dN_2}{dt}dV}{P_a} = \frac{\frac{hc}{\lambda} \int \frac{dN_2}{dt}dV}{P_a} \tag{3.109}$$

where N_2 denotes upper level population, P_a denotes the absorbed solar pump power.

Photons absorbed in a pump manifold may bypass the upper laser manifold by radiative decay to a manifold that is lower. In all probability, the decay from the pump to the upper laser manifold occurs by non-radiative transitions. If the upper laser manifold is directly below the pump manifold, the quantum efficiency is approximately [12].

$$\eta_Q = \frac{\frac{1}{\tau_{NR}}}{\left[\frac{1}{\tau_{NR}} + \frac{1}{\tau_{RAD}}\right]} \tag{3.110}$$

where τ_{NR} and τ_{RAD} are the pump manifold non-radiative and radiative lifetimes, respectively.

Quantum Defect Efficiency $\eta_S(\lambda)$, also called Stokes factor, is the ratio of the photon energy emitted at the laser transition, to the energy of a pump photon [11].

$$\eta_s = \frac{h\nu_L}{h\nu_p} = \frac{\lambda_p}{\lambda_L} \tag{3.111}$$

where: λ_p and λ_L are the pump transition and laser wavelengths, respectively.

In solar-pumped solid-sate lasers, the pump wavelength is defined as the mean absorbed and intensity-weighted solar radiation wavelength [15]

$$\lambda_p = \frac{\int_{\lambda_1}^{\lambda_2} I(\lambda)\lambda \, d\lambda}{\int_{\lambda_1}^{\lambda_2} I(\lambda)d\lambda} \tag{3.112}$$

where the integration is performed over the laser absorption bands between λ_1 and λ_2 and $I(\lambda)$ is the standard solar spectral irradiance, as shown in Fig. 3.18.

Since the laser wavelength of Nd:YAG laser material is $\lambda_L = 1064$ nm for solar-pumped Nd:YAG laser, $\lambda_P = 660$ nm was calculated by (3.112), $\eta_S = 0.62$ quantum defect efficiency is calculated for the Nd:YAG emission wavelength of $\lambda_L = 1064$ nm by (3.111).

Typically, upper state efficiencies of a Nd:YAG medium show a variation of $\eta_U(\lambda)$ from 0.58 to 0.60 [11], revealing its slight dependence on laser rod diameter. Consequently, upper state efficiency of $\boldsymbol{\eta_U(\lambda) = 0.59}$ is adopted in the following sections.

3.22 Beam Overlap Efficiency

Beam Overlap Efficiency $\boldsymbol{\eta_B}$ expresses the spatial overlap between the laser resonator modes and the pumped region of the laser medium, which can be given by an overlap integral [11].

$$\eta_B = \frac{\left(\iiint \varepsilon(x, y, z)\omega(x, y, z)dV\right)^2}{\iiint \varepsilon(x, y, z)^2\omega(x, y, z)dV} \tag{3.113}$$

where

$$\varepsilon(x, y.z) = \frac{\rho(x, y, z)}{\rho_0} \tag{3.114}$$

$\rho(x, y, z)$ is cavity mode energy density and ρ_0 is the total value of the energy density.

$$\iiint \omega(x, y, z) dV = 1 \tag{3.115}$$

$$\omega(x, y.z) = \frac{W_p(x, y, z)}{W_{p0}} \tag{3.116}$$

$W_p(x, y, z)$ denotes the pump rate per unit volume, W_{p0} is the total number of absorbed photons.

The relation between pump rate and absorbed power is given by

$$\iiint W_p(x, y, z) dV = \frac{P_a}{h\nu_p} \tag{3.117}$$

Choice of laser geometry can have a profound effect on overlap efficiency and average power capability. Historically, laser geometries were often in the form of cylinders. They can also be useful for end pumping of laser materials with low absorption coefficients. Laser rods pose a hard aperture making extraction of the population inversion near the periphery of the laser rod more difficult. If laser operation is restricted to TEM$_{00}$ modes, the beam radius is often set at about 0.6 of the laser rod radius. This restricts the overlap efficiency to roughly 0.36 [12].

In addition, cooling was usually achieved by flowing coolant over the lateral surface of the laser rod. This leads to radial thermal gradients and thermal lensing that degrades beam quality and limits average power.

Consequently, analytical calculation of the beam overlap efficiency of a solid-state laser by (3.113) is rather complex, since it is strongly dependent on the resonator parameters such as radius of curvature of cavity mirrors, cavity length, rod diameter and, more importantly, also on solar pumping conditions such as tracking errors of either a heliostat or a solar tracker in the case of solar-pumped lasers.

Therefore, it is very important to note that laser output power from a resonant cavity with a certain length L presents usually a considerably reduced laser output power level due to the influence of the beam overlap efficiency of less than unity ($\eta_B < 1$), as compared to that of a closely coupled laser resonant cavity with $\eta_B = 1$. Zemax® and LASCAD™ analyses of laser output power from a laser cavity with a certain length L was presented in Sect. 2.3 of Chap. 2. Detailed examples will also be provided in Sect. 6.2 of Chap. 6.

Finally, it is important to note that in the pump rate and the solar laser output power analysis in the following sections, $\eta_B = 1$ is usually assumed, corresponding to a laser cavity with HR and PR mirrors closely positioned near the laser rod, allowing the maximum extraction of laser power from that rod.

3.23 Atom Number Density and Solar Pump Rate Calculations

By considering a solar laser collection and concentration system with concentration factor C, the concentrated solar spectral irradiance $I'(\lambda)$ incident on the laser rod surface can be calculated

$$I'(\lambda) = \eta_T(\lambda)I(\lambda)C \tag{3.118}$$

where $I(\lambda)$ is the one-Sun solar spectral irradiance, as indicated by Fig. 3.18. $\eta_T(\lambda)$ is the solar power transfer efficiency from the primary solar collector to the surface of the laser medium.

The absorbed photon number by the laser rod with diameter D and effective absorption length L can hence be calculated

$$N_a = \pi Dl \times \int \frac{I'(\lambda)}{h\nu_p(\lambda)}\{1 - exp[-\alpha(\lambda)L]\}d\lambda \tag{3.119}$$

$$= \pi Dl \times \int \frac{\eta_T(\lambda)I(\lambda)C}{h\nu_p(\lambda)}\{1 - exp[-\alpha(\lambda)L]\}d\lambda \tag{3.120}$$

Atom number density N_U (unit $\frac{1}{cm^3}$) in the upper laser level can be calculated by considering upper state efficiency $\eta_U(\lambda)$ and laser rod volume

$$N_U = \frac{1}{\pi\left(\frac{D}{2}\right)^2 l} \times \pi Dl \times \int \frac{\eta_T(\lambda)I(\lambda)C}{h\nu_p(\lambda)}\eta_U(\lambda)\{1 - exp[-\alpha(\lambda)L]\}d\lambda \tag{3.121}$$

Since $\eta_T(\lambda)$ varies only slightly with wavelength λ within each simplified absorption band in Fig. 3.21 in Sect. 3.2, atom number density N_U in upper laser level can be finally obtained

$$N_U = \eta_T \times \frac{4C}{D} \times \int \frac{I(\lambda)}{h\nu_p(\lambda)}\eta_U(\lambda)\{1 - exp[-\alpha(\lambda)L]\}d\lambda \tag{3.122}$$

In the calculation of the output power, one of the most important parameters is the pump rate W_p. By dividing the atom number density N_U in the upper level by the total number density of the active ions in the laser rod N_t (for 1.0 at.% $Nd^{3+}YAG$ medium, $N_t = 1.38 \times 10^{20}$ cm^{-3}), the pump rate W_p can then be calculated

$$W_p = \frac{N_U}{N_t} = \eta_T \times \frac{4C}{N_t D} \times \int \frac{I(\lambda)}{h\nu_p(\lambda)}\eta_U(\lambda)\{1 - exp[-\alpha(\lambda)L]\}d\lambda \tag{3.123}$$

3.24   Solar Laser Output Power Calculation

The laser output power P_{out} of a continuous-wave laser is calculated from the following relation

$$P_{out} = \left[photon\ density\right] \times \left[lasing\ volume\ in\ the\ cavity\right]$$
$$\times \left[photon\ loss\ rate\ through\ output\ mirror\right] \times \left[photon\ energy\right] \quad (3.124)$$

and

$$V = AL' \quad (3.125)$$

where V is defined as lasing volume in the cavity, where A is the laser beam cross section, and L' is the effective cavity length

$$L' = L_C + (n - 1)l \quad (3.92)$$

Since photon loss rate through output mirror is presented by the third term on the right-hand side of (3.94)

$$P_{out} = \rho \times AL' \times \frac{c}{2L'} ln \frac{1}{R_2} \times h\nu \quad (3.126)$$

Photon loss rate through output mirror is also defined as laser power extraction efficiency.

Extraction Efficiency η_E

Laser extraction efficiency is determined by (3.127)

$$\eta_E = \frac{c}{2L'} ln \frac{1}{R_2} \quad (3.127)$$

By applying photon density ρ of (3.100)

$$P_{out} = \frac{1}{\sigma c}\left[\left(\frac{N_t \sigma l}{\gamma} - 1\right)W_p - \frac{1}{\tau_e}\right] \times AL' \times \frac{c}{2L'} ln \frac{1}{R_2} \times h\nu \quad (3.128)$$

$$= \frac{Ah\nu}{\sigma}\left(\frac{N_t \sigma l}{\gamma} - 1\right)\frac{1}{2}ln\frac{1}{R_2}\left[W_p - \frac{1}{\tau_e\left(\frac{N_t \sigma l}{\gamma} - 1\right)}\right] \quad (3.129)$$

Since normally, $\frac{N_t \sigma l}{\gamma} \gg 1$, we can reach a simplified equation for P_{out}

$$P_{out} = Ah\nu\left(\frac{N_t l}{\gamma}\right)\frac{1}{2}ln\frac{1}{R_2}\left[W_p - \frac{\gamma}{\sigma \tau_e N_t l}\right] \quad (3.130)$$

We then reach a simplified presentation for laser output power

$$P_{out} = \eta'_s \left(W_p - W_{pth} \right) \tag{3.131}$$

where: η'_s is defined as laser slope efficiency

$$\eta'_s = Ah\nu \left(\frac{N_t l}{\gamma} \right) \frac{1}{2} ln \frac{1}{R_2} \tag{3.132}$$

W_{pth} is defined as threshold pump rate.

$$W_{pth} = \frac{\gamma}{\sigma \tau_e N_t l} \tag{3.133}$$

From (3.133), it is important to note that W_{pth} is directly proportional to resonant cavity loss γ, and inversely proportional to the product of four important laser gain parameters, e.g. stimulated emission cross section σ, upper level lifetime τ_e, active ion number N_t and laser rod length l. Consequently, threshold pump rate can be either reduced by diminishing γ or by increasing σ, τ_e, N_t, l values.

By considering solar concentration ratio definition.

$$C = \frac{S_a}{S_r} = \frac{S_a}{\pi D l} \tag{3.101}$$

Incoming solar laser can be calculated by (3.134)

$$P_{in} = S_a I_0 = \pi D l C I_0 \tag{3.134}$$

where I_0 is the one-sun solar insolation in unit of power per unit area (Standard one-Sun irradiance value: $I_0 = 1000 \frac{W}{m^2}$).

Solar power to laser power conversion efficiency can then be calculated

$$\eta_c = \frac{P_{out}}{P_{in}} = \frac{P_{out}}{\pi D l C I_0} = Ah\nu \left(\frac{N_t l}{\gamma} \right) \frac{1}{2} ln \frac{1}{R_2} \left[W_p - \frac{\gamma}{\sigma \tau_e N_t l} \right] \frac{1}{\pi D l I_0 C}$$
$$= \eta'_s (W_p - W_{pth}) \frac{1}{\pi D l I_0 C} \tag{3.135}$$

Maximum pump power to threshold pump power ratio is defined

$$\frac{P_{in}}{P_{th}} = \frac{W_p}{W_{th}} = x \tag{3.136}$$

Solar laser slope efficiency can also be calculated

$$\eta_{slope} = \frac{P_{out}}{P_{in} - P_{th}} = \frac{P_{out}}{P_{in}} \frac{1}{1 - \frac{P_{th}}{P_{in}}} = \frac{P_{out}}{P_{in}} \frac{1}{1 - \frac{W_{th}}{W_p}} = \eta_c \frac{x}{x - 1} \tag{3.137}$$

3.25 Solar Spectral Irradiance and Simplified Model for Nd:YAG Absorption Spectrum

As shown in Fig. 3.21, the absorption spectra of Nd:YAG laser materials are rather complex. The absorption curve is composed of a couple of bands. Moreover, each band has a complex structure. Consequently, the analytical estimation of the pump rate by unit solar constant is rather difficult.

We therefore modeled the adsorption curves of the Nd:YAG laser material for the convenience of calculation. Five simplified absorption bands centered at 530 nm, 580 nm, 750 nm, 810 nm and 860 nm along with their respective absorption band-widths of 28 nm, 28 nm, 31 nm, 33 nm, and 22 nm respectively (green color numbers in Fig. 3.21) are considered.

A simplified absorption coefficient value $\sigma_a\left(\frac{\lambda_a + \lambda_b}{2}\right)$ for each band is assumed, corresponding to 40% of the peak absorption coefficient of that band, so that the area under the modelled absorption curve (black color) could be equal to that under the real absorption curve (blue color) in each band, as shown in Fig. 3.22.

Consequently, simplified absorption coefficients 1.39 cm^{-1}, 2.87 cm^{-1}, 3.11 cm^{-1}, 3.64 cm^{-1} and 1.23 cm^{-1} are determined for 530 nm, 580 nm, 750 nm, 810 nm and 860 nm bands, respectively, as indicated by Fig. 3.21. Correspondingly, 1.35 W/m^2/nm, 1.31 W/m^2/nm, 1.12 W/m^2/nm, 1.00 W/m^2/nm, 0.87 W/m^2/nm solar
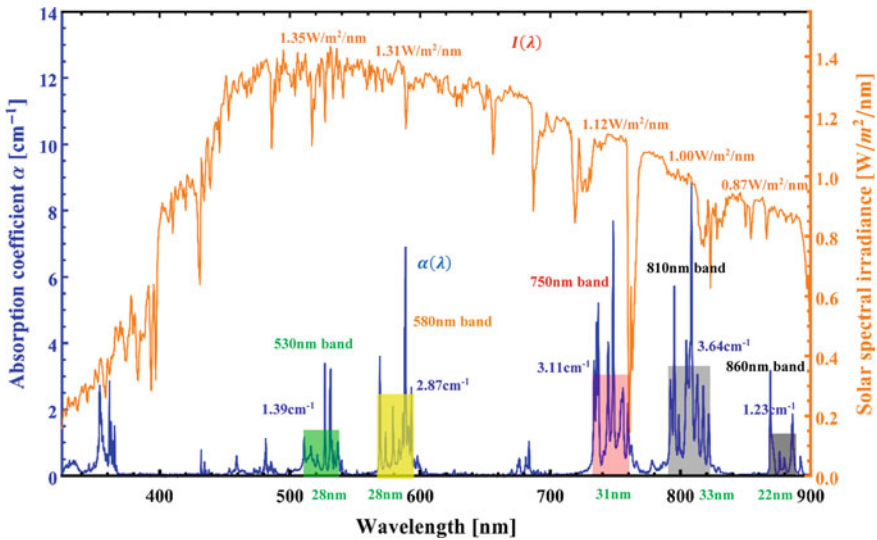

Fig. 3.21 Solar spectral irradiance and complex absorption spectra of 1.0 at.% Nd:YAG medium are presented by orange and blue lines, respectively. Five simplified absorption bands (530 nm, 580 nm, 750 nm, 810 nm and 860 nm) and their respective bandwidth (28 nm, 28 nm, 31 nm, 33 nm, and 22 nm) are indicated
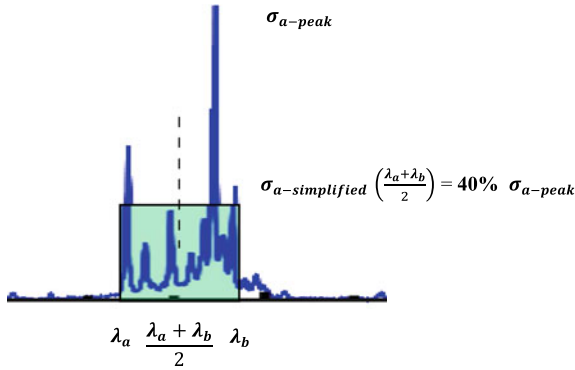
Fig. 3.22 Simplified rectangular absorption band (light green color) centered at $\frac{\lambda_a+\lambda_b}{2}$. The simplified band is limited by the minimum wavelength λ_a and the maximum wavelength λ_b. Simplified absorption coefficient corresponds to 40% of the peak absorption coefficient value of that band $\sigma_a\left(\frac{\lambda_a+\lambda_b}{2}\right) = 40\% \, \sigma_{a-peak}$

irradiance values are found to match the five simplified absorption bands centered at 530 nm, 580 nm, 750 nm, 810 nm and 860 nm, respectively.

Other absorption band of the Nd:YAG medium at UV wavelength in Fig. 3.21 is not considered since it does not contribute to 1064 nm laser emission process.

3.26   Absorbed Solar Power Density and Absorbed Pump Photon Number Density Calculations

To calculate absorbed solar power density and photon number density in each of the five simplified absorption band, as shown in Fig. 3.21, the following parameters are assumed constant within each of the simplified absorption band.

$$I(\lambda) = I\left(\frac{\lambda_a + \lambda_b}{2}\right) \; Constant\ solar\ spectral\ irradiance\ for\ each\ band \quad (3.138)$$

$$\eta_U(\lambda) = \eta_U\left(\frac{\lambda_a + \lambda_b}{2}\right) \; Constant\ upper\ state\ efficiency\ for\ each\ band \quad (3.139)$$

$$\sigma_a(\lambda) = \sigma_a\left(\frac{\lambda_a + \lambda_b}{2}\right)$$
$$= 40\,\%\,\sigma_{a-peak} \; Constant\ absorption\ coefficient\ for\ each\ band \quad (3.140)$$

Consequently, the absorption integral $\int I(\lambda)\eta_U(\lambda)\{1 - exp[-\sigma_a(\lambda)L]\}d\lambda$ for each of the five absorption band can be simplified as

$$= I\left(\frac{\lambda_a + \lambda_b}{2}\right)\eta_U\left(\frac{\lambda_a + \lambda_b}{2}\right)\left\{1 - exp\left[-\sigma_a\left(\frac{\lambda_a + \lambda_b}{2}\right)L\right]\right\}\int_{\lambda_a}^{\lambda_b} d\lambda \quad (3.141)$$

$$= I\left(\frac{\lambda_a + \lambda_b}{2}\right)\eta_U\left(\frac{\lambda_a + \lambda_b}{2}\right)\left\{1 - exp\left[-\sigma_a\left(\frac{\lambda_a + \lambda_b}{2}\right)L\right]\right\}(\lambda_b - \lambda_a) \quad (3.142)$$

We then reach a simplified equation for calculating the absorbed solar power density within each band with $\Delta\lambda = \lambda_b - \lambda_a$ bandwidth.

Absorbed solar power density in each band

$$= I\left(\frac{\lambda_a + \lambda_b}{2}\right)\eta_U\left(\frac{\lambda_a + \lambda_b}{2}\right)\left\{1 - exp\left[-\sigma_a\left(\frac{\lambda_a + \lambda_b}{2}\right)L\right]\right\}\Delta\lambda \qquad (3.143)$$

Absorbed photon number density in each band may also be simplified according the constant parameter conditions of (3.138), (3.139) and (3.140).

Simplification of integral $\int \frac{I(\lambda)}{h v_p(\lambda)}\eta_U(\lambda)\{1 - exp[-\alpha(\lambda)L]\}d\lambda$ for each band

$$= \frac{1}{h}I\left(\frac{\lambda_a + \lambda_b}{2}\right)\eta_U\left(\frac{\lambda_a + \lambda_b}{2}\right)\left\{1 - exp\left[-\sigma_a\left(\frac{\lambda_a + \lambda_b}{2}\right)L\right]\right\}\int_{\lambda_a}^{\lambda_b}\frac{1}{v_p(\lambda)}d\lambda$$

$$= \frac{1}{h}I\left(\frac{\lambda_a + \lambda_b}{2}\right)\eta_U\left(\frac{\lambda_a + \lambda_b}{2}\right)\left\{1 - exp\left[-\sigma_a\left(\frac{\lambda_a + \lambda_b}{2}\right)L\right]\right\}\int_{\lambda_a}^{\lambda_b}\frac{\lambda_p}{c}d\lambda$$

$$= \frac{1}{hc}I\left(\frac{\lambda_a + \lambda_b}{2}\right)\eta_U\left(\frac{\lambda_a + \lambda_b}{2}\right)\left\{1 - exp\left[-\sigma_a\left(\frac{\lambda_a + \lambda_b}{2}\right)L\right]\right\}\frac{(\lambda_b^2 - \lambda_a^2)}{2}$$

$$= \frac{1}{h\frac{c}{\frac{\lambda_a + \lambda_b}{2}}}I\left(\frac{\lambda_a + \lambda_b}{2}\right)\eta_U\left(\frac{\lambda_a + \lambda_b}{2}\right)\left\{1 - exp\left[-\sigma_a\left(\frac{\lambda_a + \lambda_b}{2}\right)L\right]\right\}\Delta\lambda \quad (3.144)$$

Absorbed photon number density in each absorption band is finally calculated

$$= \frac{1}{hv\left(\frac{\lambda_a + \lambda_b}{2}\right)}I\left(\frac{\lambda_a + \lambda_b}{2}\right)\eta_U\left(\frac{\lambda_a + \lambda_b}{2}\right)\left\{1 - exp\left[-\sigma_a\left(\frac{\lambda_a + \lambda_b}{2}\right)L\right]\right\}\Delta\lambda$$
$$(3.145)$$

3.27 Output Power Analysis of a Side-Pumped Nd:YAG Solar Laser

3.27.1 Modified Analytical Method for the Side-Pumped Nd:YAG Solar Laser

An astigmatic corrected target aligned (ACTA) primary parabolic mirror with S_a = 6.85 m^2 collection area was used to both collect and concentrate incoming solar power to a single-stage 2-dimensional compound parabolic concentrator (2D-CPC)
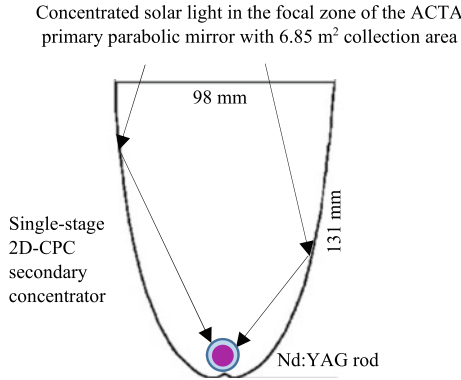
Fig. 3.23 The cross-sectional profile of the single-stage two-dimensional compound parabolic concentrator (2D-CPC). Concentrated solar lights in the focal zone were reflected to the Nd:YAG rod within the flow tube via the 2D-CPC secondary concentrator. Definite laser resonant cavity length $L = 430$ mm was adopted [16]

with 8.9 cm $\times$ 9.8 cm rectangular input face. A $D = 10$ mm diameter and $l = 130$ mm length 1.1% Nd:YAG laser rod was mounted inside a quartz flow tube, which was located along the 2D-CPC axis, as depicted in Fig. 3.23 [16].

Solar concentration ratio C

Absorbed pump power distribution of the Nd:YAG laser rod is presented by Fig. 3.24.

Since only 10 cm length of the laser rod is exposed to concentrated solar radiation within the 2D CPC pump cavity, the surface area of this exposed section of the rod is considered as a receiver, consequently.

$$S_r = \pi DL_e = 3.14 \times 1.0 \times 10 = 31.4 \ (\text{cm}^2)$$

By considering $S_a = 6.75 \ \text{m}^2$ ACTA primary solar collector area, the solar concentration ratio can be calculated

$$C = \frac{S_a}{S_r} = \frac{6.75 \times 10^4 \ \text{cm}^2}{31.4 \ \text{cm}^2} = 2150 \tag{3.146}$$

Effective absorption length L

To calculate the absorption path length L of solar pump light within the 10 mm diameter, 130 mm length Nd:YAG rod in Figs. 3.23 and 3.24, eight rectangular detectors are equally spaced around the internal surface of the rod, as indicated by Fig. 3.25. As shown in Fig. 3.19, the deviation angles of α and β of the solar ray in each detector position can be detected, so that deviation angle β' and, consequently, effective pump absorption path L at each of the eight detector positions can be calculated by (3.105), (3.106), respectively.
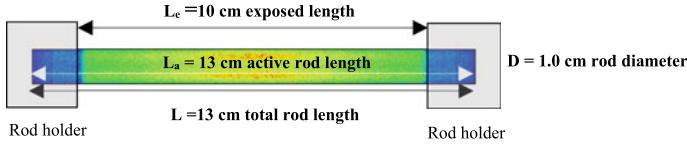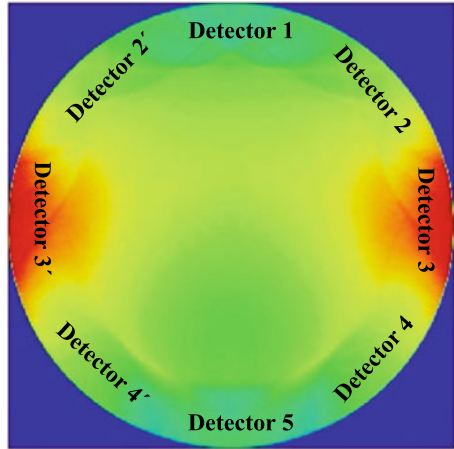
Fig. 3.24 Absorbed pump power distribution along the 10 mm diameter, 130 mm length Nd:YAG rod

Fig. 3.25 Detection of deviation angles α and β by Zemax® angle-space method. Eight detectors are positioned in equal space beneath the rod surface. Solar pump power and incident pump ray angles at each detector position can be detected simultaneously

Figures 3.26, 3.27, 3.28, 3.29 and 3.30 below show the Zemax® non-sequential ray tracing results of angle space distribution obtained from each detector rectangle. Deviation angles α and β are determined by cross section row FWHM X-coordinate value and cross section column FWHM Y-coordinate value of detectors 1–5, respectively.

Since the 2D-CPC secondary concentrator ensures a symmetric pump profile for the rod, Detector 2′, Detector 3′ and Detector 4′ in Fig. 3.25 present the same amount of detected power, the same deviation angles of α and β, and consequently, the same absorption lengths as that of Detector 2, Detector 3 and Detector 4, respectively.

Table 3.1 summarize the detected pump power for each detector. Relative weight for each detector can also be calculated. Effective absorption length in different detector positions, ranging from L_1 to L_5, are finally listed.

Finally, weighted effective absorption length L can be finally calculated

$$L = 6.47\%L_1 + 22.66\%L_2 + 41.73\%L_3 + 20.35\%L_4 + 8.79\%L_5 = 1.27(\text{cm}) \tag{3.147}$$

Calculation of absorbed solar power and absorbed photon number density in the five bands

Once the weighted effective absorption length is calculated ($L = 1.27$ cm), the amounts of absorbed pump power density and absorbed photon density within each

ZEMAX® angle-space distribution

Detector 1

Detected power 16.72W

Deviation angles

$\alpha = 7\degree, \quad \beta = 6\degree$

$Tan\ \beta' = Cos\ \alpha\ Tan\ \beta = 0.104$

$\beta' = 5.96\degree$

Optical absorption path length

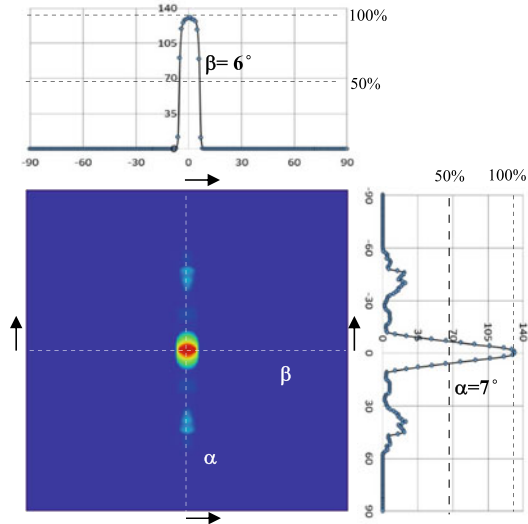$L_1 = \frac{D}{Cos\ \alpha\ Cos\ \beta'} = 1.01\ (cm)$

Fig. 3.26 Zemax® angle-space distribution of detector 1

ZEMAX® angle-space distribution

Detector 2

Detected power 29.26W

Deviation angles

$\alpha = 33\degree, \quad \beta = 3\degree$

$Tan\ \beta' = Cos\ \alpha\ Tan\ \beta = 0.044$

$\beta' = 2.52\degree$

Optical absorption path

$L_2 = \frac{D}{Cos\ \alpha\ Cos\ \beta'} = 1.19\ (cm)$
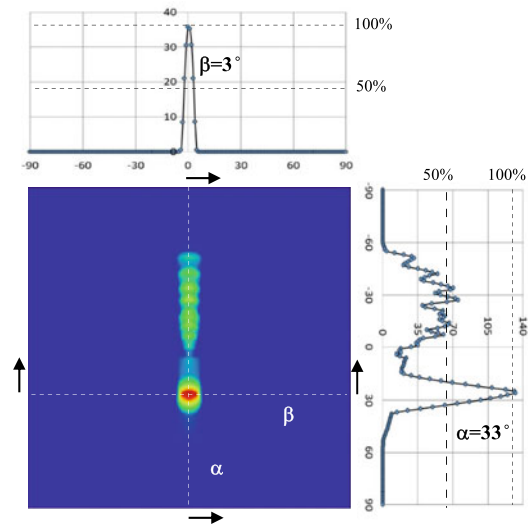
Fig. 3.27 Zemax® angle-space distribution of detector 2

of the five simplified absorption band in Fig. 3.21 can be finally calculated by using (3.143) and (3.145).

It is also important to note that simplified absorption coefficient of each band corresponds to 40% of the peak absorption coefficient value of that band $\sigma_a\left(\frac{\lambda_a+\lambda_b}{2}\right)$ = 40% σ_{a-peak}, as indicated in Fig. 3.21 by blue color text.

ZEMAX® angle-space distribution

Detector 3

Detected power 53.89W

Deviation angles

$\alpha = 39°$, $\beta = 6°$

$Tan\, \beta' = Cos\, \alpha\, Tan\, \beta = 0.082$

$\beta' = 2.72°$

Optical absorption path

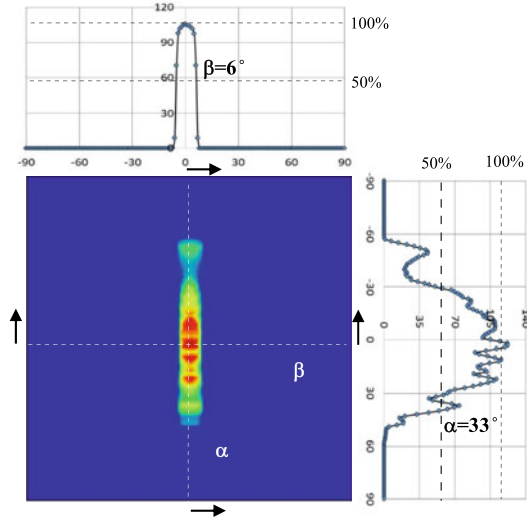$L_3 = \dfrac{D}{Cos\, \alpha\, Cos\, \beta'} = 1.29\ (cm)$

Fig. 3.28 Zemax® angle-space distribution of detector 3

ZEMAX® angle-space distribution

Detector 4

Detected power 26.28W

Deviation angles

$\alpha = 41°$, $\beta = 3°$

$Tan\, \beta' = Cos\, \alpha\, Tan\, \beta = 0.040$

$\beta' = 2.27°$

Optical absorption path

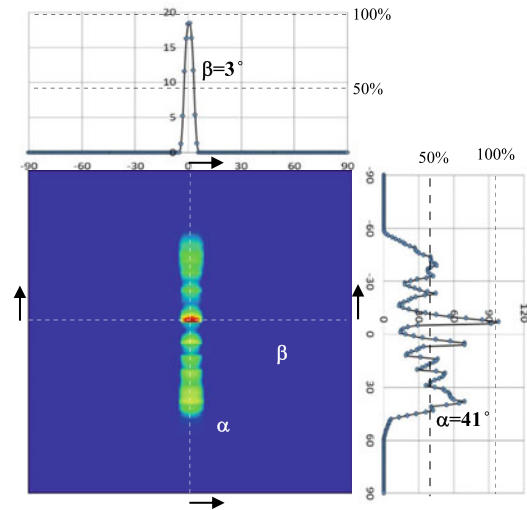$L_4 = \dfrac{D}{Cos\, \alpha\, Cos\, \beta'} = 1.33(cm)$

Fig. 3.29 Zemax® angle-space distribution of detector 4

By adopting Eq. (3.143):

$$I\left(\frac{\lambda_a + \lambda_b}{2}\right)\left\{1 - exp\left[-\sigma_a\left(\frac{\lambda_a + \lambda_b}{2}\right)L\right]\right\}\Delta\lambda$$

ZEMAX® angle-space distribution

Detector 5

Detected power 22.72W

Deviation angles

$\alpha = 44°$, $\beta = 6°$

$Tan\ \beta' = Cos\ \alpha\ Tan\ \beta = 0.076$

$\beta' = 4.32°$

Optical absorption path

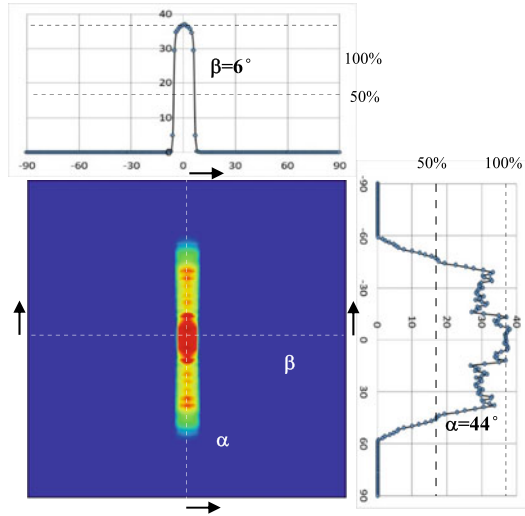$L_5 = \dfrac{D}{Cos\ \alpha\ Cos\ \beta'} = 1.39\ (cm)$

Fig. 3.30 Zemax® angle-space distribution of detector 5

Table 3.1 Effective absorption lengths determined by the deviation angles of 8 detectors. Since each detector detect different amount of solar pump power, different weight are calculated accordingly, indicating non-homogeneous solar pumping around the laser rod, as indicated by Fig. 3.25

	Detected solar pump power (W)	Weight (%)	Effective absorption length (cm)
Detector 1	16.72	6.47	$L_1 = 1.01$
Detectors 2 + 2′	$2 \times 29.26 = 58.52$	22.66	$L_2 = 1.19$
Detectors 3 + 3′	$2 \times 53.89 = 107.78$	41.73	$L_3 = 1.29$
Detectors 4 + 4′	$2 \times 26.28 = 52.56$	20.35	$L_4 = 1.33$
Detector 5	22.72	8.79	$L_5 = 1.39$
	Total detected power 258.30 W	100.00	Weighted absorption length L = 1.27 cm

Absorbed solar pump power density in 530 nm band can be calculated

$$= I(530\ nm)\{1 - \exp[-\alpha_a(530\ nm)L]\}28\ nm$$

$$= 1.35\frac{W}{m^2 nm}\{1 - \exp[-1.53\ cm^{-1} \times 1.27\ cm]\}28\ nm$$

$$= 32.40\ \frac{W}{m^2}$$

By adopting Eq. (3.145):

$$\frac{1}{h\upsilon\left(\frac{\lambda_a + \lambda_b}{2}\right)}I\left(\frac{\lambda_a + \lambda_b}{2}\right)\left\{1 - \exp\left[-\sigma_a\left(\frac{\lambda_a + \lambda_b}{2}\right)L\right]\right\}\Delta\lambda$$

Absorbed solar photon number density in 530 nm band can also be calculated

$$= \frac{32.40\frac{W}{m^2}}{h\upsilon(530 \text{ nm})} = \frac{32.40\frac{W}{m^2}}{3.75 \times 10^{-19} \text{ J}} = 0.864 \times 10^{20}\frac{1}{m^2s}$$

In the same way, absorbed solar pump power density in 580 nm band

$$= I(580 \text{ nm})\{1 - \exp[-\alpha_a(580 \text{ nm})L]\}28 \text{ nm}$$
$$= 1.31\frac{W}{m^2nm}\left\{1 - \exp\left[-3.16 \text{ cm}^{-1} \times 1.27 \text{ cm}\right]\right\}28 \text{ nm}$$
$$= 36.02\frac{W}{m^2}$$

Absorbed solar photon number density in 580 nm band

$$= \frac{36.02\frac{W}{m^2}}{h\upsilon(580 \text{ nm})} = \frac{36.02\frac{W}{m^2}}{3.43 \times 10^{-19} \text{ J}} = 1.050 \times 10^{20}\frac{1}{m^2s}$$

Absorbed solar pump power density in 750 nm band

$$= I(750 \text{ nm})\{1 - \exp[-\alpha_a(750 \text{ nm})L]\}31 \text{ nm}$$
$$= 1.12\frac{W}{m^2nm}\left\{1 - \exp\left[-3.42 \text{ cm}^{-1} \times 1.27 \text{ cm}\right]\right\}31 \text{ nm}$$
$$= 34.27\frac{W}{m^2}$$

Absorbed solar photon number density in 750 nm band

$$= \frac{34.27\frac{W}{m^2}}{h\upsilon(750 \text{ nm})} = \frac{34.27\frac{W}{m^2}}{2.65 \times 10^{-19} \text{ J}} = 1.293 \times 10^{20}\frac{1}{m^2s}$$

Absorbed solar pump power density in 810 nm band

$$= I(810 \text{ nm})\{1 - \exp[-\alpha_a(810 \text{ nm})L]\}33 \text{ nm}$$
$$= 1.00\frac{W}{m^2nm}\left\{1 - \exp\left[-4.00 \text{ cm}^{-1} \times 1.27 \text{ cm}\right]\right\}33 \text{ nm}$$
$$= 32.80\frac{W}{m^2}$$

Absorbed solar photon number density in 810 nm band

$$= \frac{32.80\frac{W}{m^2}}{h\upsilon(810 \text{ nm})} = \frac{32.80\frac{W}{m^2}}{2.45 \times 10^{-19} \text{ J}} = 1.339 \times 10^{20}\frac{1}{m^2s}$$

Absorbed solar pump power density in 860 nm band

$$= I(860 \text{ nm})\{1 - \exp[-\alpha_a(860 \text{ nm})L]\}22 \text{ nm}$$

$$= 0.87 \frac{\text{W}}{\text{m}^2\text{nm}}\{1 - \exp[-1.35 \text{ cm}^{-1} \times 1.27 \text{ cm}]\}22 \text{ nm}$$

$$= 15.71 \frac{\text{W}}{\text{m}^2}$$

Absorbed solar photon number density in 860 nm band

$$= \frac{15.71 \frac{\text{W}}{\text{m}^2}}{h\upsilon(860 \text{ nm})} = \frac{15.71 \frac{\text{W}}{\text{m}^2}}{2.31 \times 10^{-19} \text{ J}} = 0.680 \times 10^{20} \frac{1}{\text{m}^2\text{s}}$$

Finally, we obtain the total absorbed solar power density of the five absorption bands

$$\sum_1^5 P_i = 32.40 \frac{\text{W}}{\text{m}^2} + 36.02 \frac{\text{W}}{\text{m}^2} + 34.27 \frac{\text{W}}{\text{m}^2} + 32.80 \frac{\text{W}}{\text{m}^2} + 15.71 \frac{\text{W}}{\text{m}^2}$$

$$= 151.20 \frac{\text{W}}{\text{m}^2} \tag{3.148}$$

And the total absorbed photon number density from the five bands:

$$\sum_1^5 F_i = 0.864 \times 10^{20} \frac{1}{\text{m}^2\text{s}} + 1.050 \times 10^{20} \frac{1}{\text{m}^2\text{s}}$$

$$+ 1.293 \times 10^{20} \frac{1}{\text{m}^2\text{s}} + 1.339 \times 10^{20} \frac{1}{\text{m}^2\text{s}} + 0.680 \times 10^{20} \frac{1}{\text{m}^2\text{s}}$$

$$= 5.226 \times 10^{20} \frac{1}{\text{m}^2\text{s}} = 5.226 \times 10^{16} \frac{1}{\text{cm}^2\text{s}} \tag{3.149}$$

Calculation of one sun pump rate W_p'

The astigmatic corrected target aligned (ACTA) parabolic mirror with 6.75 m² collection area was used to both collect and concentrate incoming solar power. For $950 \frac{\text{W}}{\text{m}^2}$ solar irradiance, 6412.5 W incoming solar power was calculated. By assuming infinite absorption coefficient $\alpha_a(\lambda) = \infty$, 4225.8 W absorbed power at rod surface was detected by Zemax® software.

Consequently, $\eta_T = \frac{4225.8W}{6412.5W} = 0.659$ transfer efficiency was calculated.

As discussed in Sect. 3.20, $\eta_U(\lambda) = 0.59$ upper state efficiency was assumed in our analysis [11].

Since both which $\eta_T(\lambda)$ and $\eta_U(\lambda)$ remain nearly constant within each of the five absorption bands, we then reach simplified equation for one sun pump rate

$$W_p' = \eta_T \eta_U \frac{4}{N_t D} \int \frac{I(\lambda)}{h\upsilon(\lambda)}\{1 - \exp[-\alpha(\lambda)L]\}d\lambda = \eta_T \eta_U \frac{4}{N_t D} \sum_1^5 F_i$$

$$= 0.493 \times 0.59 \times \frac{4}{1.518 \times 10^{20} \text{ cm}^{-3} \times 1.0 \text{ cm}} \times 5.226 \times 10^{16} \frac{1}{\text{cm}^2 \text{s}}$$

$$= 0.40 \times 10^{-3} \frac{1}{\text{s}} \qquad\qquad (3.150)$$

Calculation of threshold pump rate W_{pth}

For 1.1 at.% Nd:YAG rod, $\sigma = 6.5 \times 10^{-19}$ cm^2, $l = 13$ cm, $D = 1$ cm, $A = 0.785$ cm^2 $R_1 = 0.998$, $R_2 = 0.95$, $N_t = 1.518 \times 10^{20}$ cm^{-3}.

The single-trip loss of the laser resonant cavity is firstly calculated

$$\gamma = \alpha l + \frac{1}{2}\left[\ln\left(\frac{1}{R_1}\right) + \ln\left(\frac{1}{R_2}\right)\right]$$

$$= 0.003 \text{ cm}^{-1} \times 13 \text{ cm} + \frac{1}{2}\left[\ln\left(\frac{1}{0.998}\right) + \ln\left(\frac{1}{0.95}\right)\right] = 6.57\% \quad (3.151)$$

Then we can calculate the threshold solar pump rate

$$W_{pth} = \frac{\gamma}{\sigma \tau_e N_t l} = \frac{0.0657}{6.5 \times 10^{19} \text{ cm}^2 \times 230 \times 10^{-6} \text{ s} \times 1.518 \times 10^{20} \text{ cm}^{-3} \times 13 \text{ cm}}$$

$$= 0.223 \text{ s}^{-1} \qquad\qquad (3.152)$$

Calculation of solar laser output power

$$P_{out} = Ah\upsilon\left(\frac{N_t l}{\gamma}\right)\frac{1}{2}\ln\frac{1}{R_2}\left[CW_p' - \frac{\gamma}{\sigma \tau_e N_t l}\right]$$

$$= 0.785 \text{ cm}^2 \times 6.63 \times 10^{-34} \text{ J S} \times 2.82 \times 10^{14} \text{ S}^{-1}$$

$$\times \left(\frac{1.518 \times 10^{20} \text{ cm}^{-3} \times 13 \text{ cm}}{0.0657}\right)\frac{1}{2}\ln$$

$$\times \frac{1}{0.95}\left(2150 \times 0.40 \times 10^{-3}\frac{1}{\text{s}} - 0.223\frac{1}{\text{s}}\right) = \eta_s'\left(CW_p' - W_{pth}\right)$$

$$= 113.1\text{J}\left(0.860 \text{ S}^{-1} - 0.223 \text{ S}^{-1}\right) = 72.0 \text{ W} \qquad (3.153)$$

Calculation of $\frac{P_{in}}{P_{pth}}$ ratio

$$x = \frac{P_{in}}{P_{pth}} = \frac{W_p}{W_{pth}} = \frac{CW_p'}{W_{pth}} = \frac{0.860 \text{ S}^{-1}}{0.223 \text{ S}^{-1}} = 3.86 \qquad (3.154)$$

Calculation of threshold pump power P_{pth}

$$P_{pth} = \frac{P_{in}}{x} = \frac{6412.5 \text{ W}}{3.86} = 1661.3 \text{ W} \tag{3.155}$$

Calculation of solar to laser power conversion efficiency η

With 6.75 m^2 collection area, at 950 W/m^2 solar irradiance, 6412.5 W incoming solar power is calculated.

$$\eta = \frac{P_{out}}{P_{in}} = \frac{72.0 \text{ W}}{6412.5 \text{ W}} = 1.12\% \tag{3.156}$$

Calculation of solar laser slope efficiency η_{slope}

$$\eta_{slope} = \frac{P_{out}}{(P_{in} - P_{th})} = \frac{P_{out}}{P_{in}\left(1 - \frac{P_{th}}{P_{in}}\right)} = \eta \frac{1}{\left(1 - \frac{1}{x}\right)}$$

$$= \eta \frac{x}{x-1} = 1.12\% \frac{3.86}{3.86 - 1} = 1.51\% \tag{3.157}$$

3.27.2 Classical Analytical Method of Side-Pumped Solar Laser

The following equations are commonly used classical analytical method for calculating laser output power P_{out}, slope efficiency η_s and threshold pump power P_{th} of solid-state lasers [2].

$$P_{out} = \frac{1-R}{1+R}\left(\frac{2\eta_{OVP}\eta_T\eta_A\eta_U\eta_B}{\delta - lnR}P_{in} - AI_s\right) \tag{3.158}$$

$$\eta_s = \frac{1-R}{1+R}\left(\frac{2\eta_{OVP}\eta_T\eta_A\eta_U\eta_B}{\delta - lnR}\right) \tag{3.159}$$

$$P_{th} = \frac{\delta - lnR}{2\eta_{OVP}\eta_T\eta_A\eta_U\eta_B}AI_s \tag{3.160}$$

where:

$$I_s = \frac{h\upsilon}{\tau\sigma} = \frac{6.63 \times 10^{-34} \text{ JS} \times 2.82 \times 10^{14} \text{ s}^{-1}}{230 \times 10^{-6} \text{ S} \times 6.5 \times 10^{-19} \text{ cm}^2} = 1.2506 \text{ kW/cm}^2$$

For the side-pumped solar laser in Fig. 3.23, all other important parameters and laser output power are calculated by (3.158), (3.159) and (3.160) and listed by Table 3.2.

Table 3.2 Design parameters and output power of the side-pumped solar laser

| Parameters	
Irradiance (W/m^2)	950
Collection area (m^2)	6.75
P_{IN} (W)	6412.5
Rod diameter (cm)	1
Length l (cm)	13
A (cm^2)	0.785
I_S (kW/cm^2)	1.2506
A I_S (W)	981.7
α (cm^{-1})	0.003
$2\alpha l$	0.078
δ_M	0.004
δ_D	0.000
$\delta = 2\alpha l + \delta_M + \delta_D$	0.082
R	0.95
(1-R)/(1 + R)	0.02564
$\delta - \ln R$	0.1333
η_{ovp}	0.16
P_{SOURCE} (Zemax) (W)	1026
$P_{TRANSFER}$ (Zemax) (W)	505.93
η_T	0.493
$P_{ABSORBED}$ (Zemax) (W)	423.58
η_A	0.837
η_U	0.59
$\eta = \eta_{OVP}\eta_T\eta_A\eta_U\eta_B$	0.03895
Analytical calculation	
P_{OUT} (W)	70.9
Total η_{SLOPE} (%)	1.50
P_{TH} (W)	1679.4
Solar-to-laser conversion efficiency (%)	0.94

3.27.3 LASCAD™ Analysis of the Side-Pumped Solar Laser

Similar to the Zemax® and LASCAD™ solar laser analysis examples in Chap. 2, the absorbed pump flux data from the Zemax® analysis of the side-pumped solar laser in Figs. 3.23 and 3.24 can be processed by LASCAD™ software to evaluate laser output performances.

The stimulated emission cross-section of 6.5×10^{-19} cm^2, the fluorescence life time of 230 μs and an absorption and scattering loss of 0.003 cm^{-1} for the 1.1

at.% Nd:YAG medium were adopted in LASCAD™ analysis. The mean absorbed and intensity-weighted solar pump wavelength of 660 nm [14] was also used in the analysis. For the 10.0 mm diameter, 1.1 at.% Nd:YAG rod with length $L_R = 130$ mm, the amount of absorption and scattering losses was $2 \, \alpha \, L_R = 5.2\%$. Assuming 0.4% of imperfect HR and AR coating losses, the round-trip loss was increased to 5.6%. The diffraction losses depend heavily on rod diameter, resonator length and RoC of the resonator mirrors. LASCAD™ beam propagation method (BPM) resulted in a negligible diffraction loss when HR1064 nm end mirror and PR1064 nm output mirror, all with RoC $= \infty$, were placed very close to the laser rod. Final round-trip loss of 5.6% was calculated. Consequently, 72.5 W multimode solar laser power was numerically calculated.

By considering the incoming solar power of 6412.5 W and for the maximum solar laser output power of 72.5 W, solar-to-laser conversion efficiency of 1.13% is calculated. Effective threshold solar pump power and maximum effective solar power of 104.4 W, 417.0 W was indicated in Fig. 3.31, respectively, corresponding to 1587.3 W threshold solar power and the maximum incoming solar power of 6412.5 W, respectively. Solar laser slope efficiency of 1.5% was hence be calculated. Maximum pump power/threshold pump power ratio of 4.04 was calculated. All the above mentioned parameters are indicated in Table 3.3.

Under the same pumping conditions for the laser resonator with L $= 430$ mm length, 45.9 W laser output power, 1687.5 W threshold pump power, 0.716% solar-to-laser conversion efficiency, 0.97% laser slope efficiency and 3.8 maximum pump power/threshold pump power ratio were calculated by LASCAD™ software, as shown in Fig. 3.32.
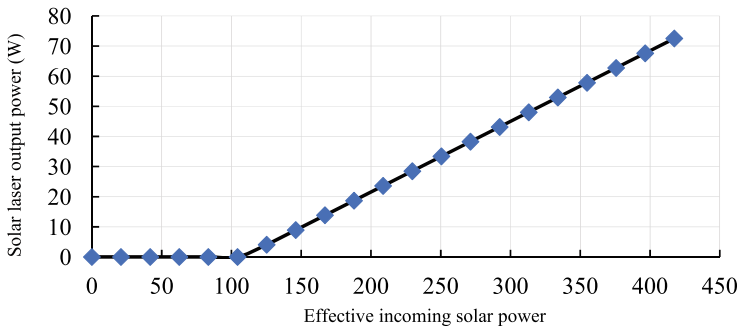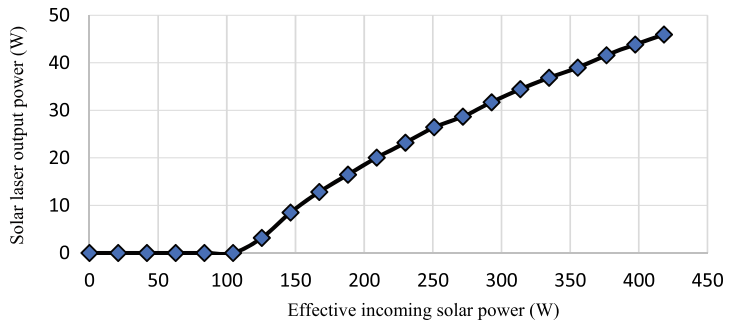

| Effective solar pump power | 104.4W | 417.0W |
| Incoming solar power | 1587.3W | 6412.5W |

Fig. 3.31 Numerically calculated solar laser output power versus effective incoming solar power by assuming a closely coupled resonant cavity

Table 3.3 Side-pumped solar laser output performance by different analysis methods

	Laser output power (W)	Threshold pump power (W)	Solar-to-laser conversion efficiency (%)	Laser slope efficiency (%)	Maximum pump power/threshold pump power ratio
Modified analysis	72.0	1661.3	1.120	1.51	3.86
Classical analysis	70.9	1680.2	1.106	1.50	3.82
LASCAD$_{Max}$	72.5	1587.3	1.130	1.50	4.04
LASCAD$_{L430mm}$	45.9	1687.5	0.716	0.97	3.80
Experimental	46.0	2596.2	0.717	1.20	2.47

| Effective solar pump power | 104.4W | 417.0W |
| Incoming solar power | 1587.3W | 6412.5W |

Fig. 3.32 Numerically calculated solar laser output power versus effective incoming solar power for the laser resonant cavity with $L = 46$ cm length

3.27.4 Comparison of Different Analysis Methods of the Side-Pumped Solar Laser

Discussions

As shown by Table 3.3, both the modified and the LASCAD™ analyses predicted nearly the same maximum extractable multimode laser power and solar-to-laser conversion efficiency when the HR1064 nm end mirror and PR1064 nm output mirrors were closely placed near the Nd:YAG laser rod. This happened when unity overlap efficiency ($\eta_B = 1$) was assumed in the modified method. Classical analytical method offered a considerably reduced prediction accuracy for laser power and efficiency, as indicated by Table 3.3.

However, it is important to note that both the modified and the classical analyses were not effective in predicting the output power from a laser resonant cavity with a certain cavity length L ($\eta_B < 1$), since it was very difficult to calculate analytically the beam overlap efficiency of solar-pumped lasers, as mentioned in Sect. 3.22.

Zemax® and LASCAD™ analyses were effective in the laser output power prediction of a solar laser with certain cavity length, as explained in Sect. 2.26 of Chap. 2. Detailed analysis method will be provided in Sect. 6.2.1 of Chap. 6.

When the HR1064 nm end mirror and the PR1064 nm output mirror were positioned 430 mm away from each other, there was a noticeable reduction in beam overlap efficiency ($\eta_B < 1$), consequently, 45.9 W solar laser output power was calculated by Zemax® and LASCAD$_{L430mm}$ analyses, as shown by Fig. 3.32 and confirmed by experimental result [16].

As for the prediction of threshold solar pump power, all the analyses including LASCAD™ failed to a considerable extent, leading normally to a much smaller threshold power prediction accuracy, as compared to the experimental result in Table 3.3.

3.28 Output Power Analysis of an End-Side-Pumped Nd:YAG Solar Laser

3.28.1 Modified Analytical Method for the End-Side-Pumped Nd:YAG Solar Laser

Solar concentration factor C

The Fresnel lens collector has the collection area of $S_A = \pi R^2 = 6358.5$ cm^2 (Fig. 3.33).

The $D = 0.4$ cm, $l = 2.1$ cm rod has an exposed surface area of $S_R = \frac{\pi D^2}{4} + \pi D l = 2.763$ cm^2.
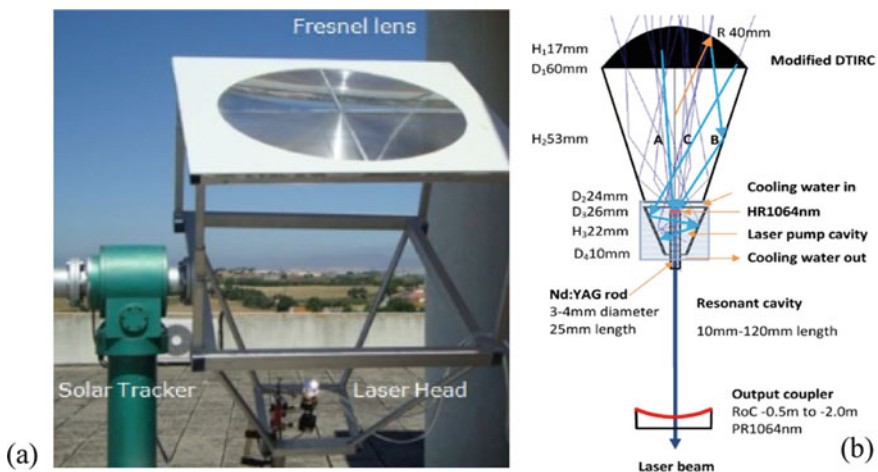

Fig. 3.33 **a** The Nd:YAG solar-pumped laser system with a 0.9 m diameter Fresnel lens and **b** a laser head positioned in the focal zone of the Fresnel lens [14]
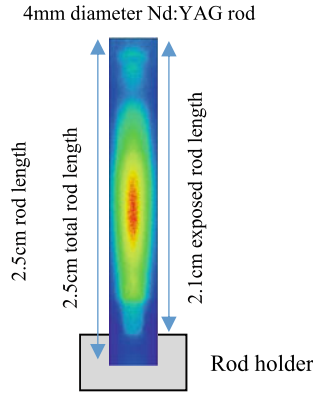
4mm diameter Nd:YAG rod

Fig. 3.34 Absorbed pump power distribution along a 4 mm diameter, 25 mm length Nd:YAG rod

The solar concentration ratio C is hence calculated:

$$C = \frac{S_A}{S_R} = 2301.3 \qquad (3.161)$$
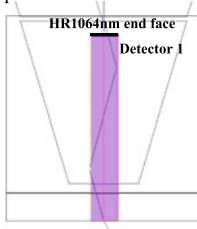
Effective absorption length L

By Zemax® analysis, 24.8% of all the solar pump ray were found to enter the D = 4 mm diameter and l = 25 mm length Nd:YAG rod through its HR1064 nm end face, ensuring the most efficient pump light absorption through end-pumping configuration. Similar to the divergence angle analysis of the solar pump rays within a laser rod in in Sect. 3.27, a square detector (Detector 1) was placed beneath the HR1064 nm end face of the D = 4 mm diameter and l = 25 mm length Nd:YAG rod, as indicated by Figs. 3.34 and 3.35. $\gamma_x = \gamma_y = 20°$ divergence angles were detected. Effective absorption length $L_{\text{End-pumping}}$ = 2.81 cm was consequently calculated.

By Zemax® analysis, 69.6% of all the solar pump ray were found to enter the D = 4 mm diameter and l = 25 mm length Nd:YAG rod through its side barrel face, ensuring also an efficient pump light absorption through three-pass side-pumping configuration, a detector rectangle (Detector 2) was placed beneath the side face of the D = 4 mm = 0.4 cm diameter and l = 25 mm length Nd:YAG rod, as indicated by Fig. 3.36. α=32°, β=21° divergence angles were detected. Effective absorption length $L_{\text{Three-pass}}$=1.39 cm was calculated. End-pumping solar pump rays in Fig. 3.35 were also detected by Detector 2.

By Zemax® analysis, only 5.6% of all the solar pump ray were found to enter the D = 4 mm diameter and l = 25 mm length rod through its side face in one-pass pumping approach, leading to an inefficient pump light absorption. A short detector rectangle (Detector 3) was placed beneath the side face of the Nd:YAG rod, as indicated by Fig. 3.37. α = 25°, β = 28° divergence angles were detected. Effective absorption length $L_{\text{One-pass}}$ = 0.49 cm was calculated. To detect the one-pass rays

ZEMAX® angle-space distribution

Detector 1

End-pumping

Deviation angles:

$\gamma_x = 20°, \ \gamma_y = 20°$

$Tan \ \beta' = Cos \ \gamma_x \ Tan \ \gamma_y = 0.342$

$\gamma' = 18.9°$

Effective absorption length:

$$L_{End-pumping} = \frac{2.5}{Cos \ \gamma_x Cos \ \gamma'}$$
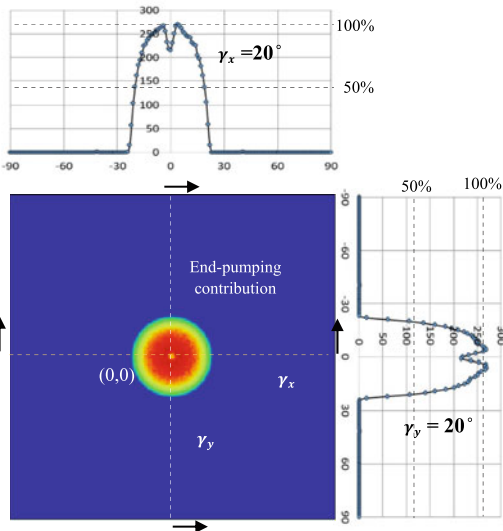$$= 2.81(cm)$$

Fig. 3.35 Zemax® angle-space distribution of detector 1 for end-pumping

ZEMAX® angle-space distribution
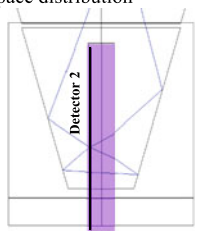
Detector 2

Side-pumping

Deviation angles

$\alpha = 32°, \beta = 21°$

$Tan \ \beta' = Cos \ \alpha \ Tan \ \beta = 0.326$

$\beta' = 18.0°$

Effective absorption length

$$L_{Three-pass} = 2 \times \frac{D}{Cos \ \alpha \ Cos \ \beta'} + 4$$
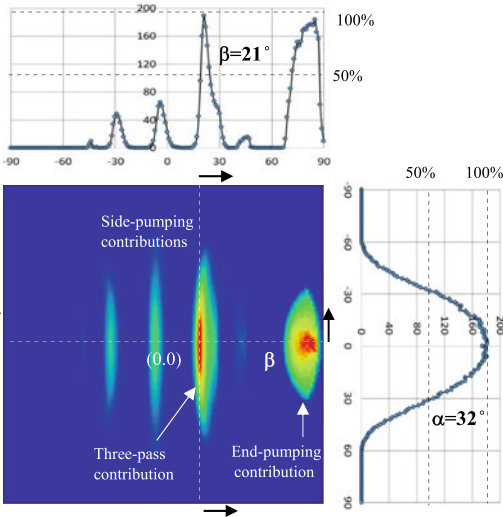$$= 1.39(cm)$$

Fig. 3.36 Zemax® angle-space distribution of detector 2 for three-pass side-pumping

more effectively, Detector 3 was positioned near the output end of the rod. Besides, since Detector 3 also had a much shorter length than that of Detector 2, contribution of the solar rays through the HR 1064 nm end face was much less pronounced in Fig. 3.37, as compared to that in Fig. 3.36.

Zemax® analysis of different effective absorption lengths and their relative weights for different passes (Table 3.4)

$$L = 24.8\% \times L_{\text{End-pumping}} + 69.6\% \times L_{\text{Three-pass}} + 5.6\% \times L_{\text{One-pass}}$$
$$= 24.8\% \times 2.81 + 69.6\% \times 1.39 + 5.6\% \times 0.49 = 1.69 \, (\text{cm}) \qquad (3.162)$$

ZEMAX® angle-space distribution

Detector 3

Side-pumping

Deviation angles

$\alpha = 25°, \beta = 28°$

Tan $\beta' =$ Cos α Tan $\beta = 0.482$

$\beta' = 25.7°$

Optical absorption path length

$$L_{One-pass} = \frac{D}{Cos\,\alpha\,Cos\,\beta'}$$
$$= 0.49 \, (cm)$$
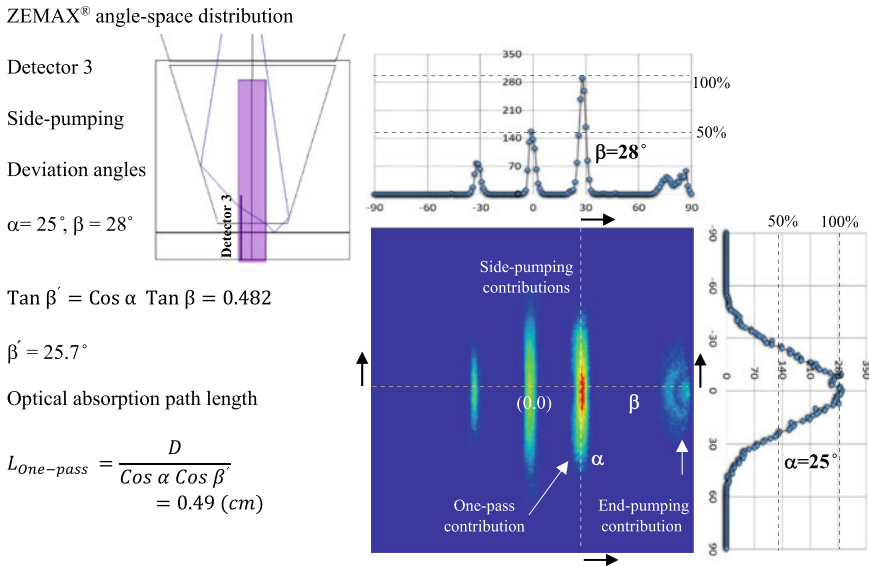
Fig. 3.37 Zemax® angle-space distribution of detector 3 for one-pass side-pumping

Table 3.4 Effective absorption length for end-side-pumping approach		End-pumping	Three-pass side pumping	One-pass side pumping
	Weight	24.8%	69.6%	5.6%
	Type	$L_{\text{End-pumping}}$	$L_{\text{Three-pass}}$	$L_{\text{One-pass}}$
	Effective absorption length	2.81 cm	1.39 cm	0.49 cm

Calculation of absorbed solar power and absorbed photon number density in the five bands

Once the weighted effective absorption length ($L = 1.69$ cm) is found, the amounts of absorbed pump power density and absorbed photon density within each of the five simplified absorption band in Fig. 3.21 can be finally calculated by using (3.143) and (3.145).

By adopting Eq. (3.143): $I\left(\frac{\lambda_a+\lambda_b}{2}\right)\left\{1 - \exp\left[-\sigma_a\left(\frac{\lambda_a+\lambda_b}{2}\right)L\right]\right\}\Delta\lambda$.

Absorbed solar pump power density in 530 nm band

$$= I(530 \text{ nm})\{1 - \exp[-\alpha_a(530 \text{ nm})L]\}28 \text{ nm}$$

$$= 1.35\frac{\text{W}}{\text{m}^2\text{nm}}\left\{1 - \exp\left[-1.39 \text{ cm}^{-1}1.69 \text{ cm}\right]\right\}28 \text{ nm}$$

$$= 34.19\,\frac{\text{W}}{\text{m}^2}$$

By adopting Eq. (3.145): $\frac{1}{h\upsilon\left(\frac{\lambda_a+\lambda_b}{2}\right)}I\left(\frac{\lambda_a+\lambda_b}{2}\right)\left\{1 - \exp\left[-\sigma_a\left(\frac{\lambda_a+\lambda_b}{2}\right)L\right]\right\}\Delta\lambda$

Absorbed solar photon density in 530 nm band

$$= \frac{34.19\frac{\text{W}}{\text{m}^2}}{h\upsilon(530 \text{ nm})} = \frac{34.19\frac{\text{W}}{\text{m}^2}}{3.75 \times 10^{-19} \text{ J}} = 0.912 \times 10^{20}\,\frac{1}{\text{m}^2\text{s}}$$

Similarly, absorbed solar pump power density in 580 nm band

$$I(580 \text{ nm})\{1 - \exp[-\alpha_a(580 \text{ nm})L]\}\ 28 \text{ nm}$$

$$= 1.31\frac{\text{W}}{\text{m}^2\text{nm}}\left\{1 - \exp\left[-2.87 \text{ cm}^{-1}1.69 \text{ cm}\right]\right\}\ 28 \text{ nm}$$

$$= 36.39\,\frac{\text{W}}{\text{m}^2}$$

Absorbed solar photon number density in 580 nm band

$$= \frac{36.39\frac{\text{W}}{\text{m}^2}}{h\upsilon(580 \text{ nm})} = \frac{36.39\frac{\text{W}}{\text{m}^2}}{3.43 \times 10^{-19} \text{ J}} = 1.061 \times 10^{20}\,\frac{1}{\text{m}^2\text{s}}$$

Absorbed solar pump power density in 750 nm band

$$I(750 \text{ nm})\{1 - \exp[-\alpha_a(750 \text{ nm})L]\}\ 31 \text{ nm}$$

$$= 1.12\frac{\text{W}}{\text{m}^2\text{nm}}\left\{1 - \exp\left[-3.11 \text{ cm}^{-1}1.69 \text{ cm}\right]\right\}\ 31 \text{ nm}$$

$$= 34.54\,\frac{\text{W}}{\text{m}^2}$$

Absorbed solar photon number density in 750 nm band

$$= \frac{34.54\frac{\text{W}}{\text{m}^2}}{h\upsilon(750 \text{ nm})} = \frac{34.54\frac{\text{W}}{\text{m}^2}}{2.65 \times 10^{-19} \text{ J}} = 1.303 \times 10^{20}\,\frac{1}{\text{m}^2\text{s}}$$

Absorbed solar pump power density in 810 nm band

$$I(810 \text{ nm})\{1 - \exp[-\alpha_a(810 \text{ nm})L]\} \, 33 \text{ nm}$$
$$= 1.00 \frac{W}{m^2 nm} \{1 - \exp[-3.64 \text{ cm}^{-1} 1.69 \text{ cm}]\} \, 33 \text{ nm}$$
$$= 32.93 \frac{W}{m^2}$$

Absorbed solar photon number density in 810 nm band

$$= \frac{32.93 \frac{W}{m^2}}{h\upsilon(810 \text{ nm})} = \frac{32.93 \frac{W}{m^2}}{2.45 \times 10^{-19} \text{ J}} = 1.344 \times 10^{20} \frac{1}{m^2 s}$$

Absorbed solar pump power density in 860 nm band

$$I(860 \text{ nm})\{1 - \exp[-\alpha_a(860 \text{ nm})L]\} \, 22 \text{ nm}$$
$$= 0.87 \frac{W}{m^2 nm} \{1 - \exp[-1.23 \text{ cm}^{-1} 1.69 \text{ cm}]\} \, 22 \text{ nm}$$
$$= 16.75 \frac{W}{m^2}$$

Absorbed solar photon number density in 860 nm band

$$= \frac{16.75 \frac{W}{m^2}}{h\upsilon(860 \text{ nm})} = \frac{16.75 \frac{W}{m^2}}{2.31 \times 10^{-19} \text{ J}} = 0.725 \times 10^{20} \frac{1}{m^2 s}$$

Finally, total absorbed solar power density from the five bands

$$\sum_1^5 P_i = 34.19 \frac{W}{m^2} + 36.39 \frac{W}{m^2} + 34.54 \frac{W}{m^2} + 32.93 \frac{W}{m^2} + 16.75 \frac{W}{m^2}$$
$$= 154.8 \frac{W}{m^2} \tag{3.163}$$

Total absorbed photon number density from the five bands

$$\sum_1^5 F_i = 0.912 \times 10^{20} \frac{1}{m^2 s} + 1.061 \times 10^{20} \frac{1}{m^2 s} + 1.303 \times 10^{20} \frac{1}{m^2 s}$$
$$+ 1.344 \times 10^{20} \frac{1}{m^2 s} + 0.725 \times 10^{20} \frac{1}{m^2 s} = 5.345 \times 10^{20} \frac{1}{m^2 s}$$
$$= 5.345 \times 10^{16} \frac{1}{cm^2 s} \tag{3.164}$$

Calculation of one Sun pump rate W'_p

For the Fresnel lens with 0.63585 m^2 collection area and 890 $\frac{W}{m^2}$ solar irradiance, 565.9 W incoming solar power was calculated. By assuming infinite absorption

coefficient $\alpha_a(\lambda) = \infty$, 372.9 W absorbed solar power at rod surface was detected by Zemax® software.

Consequently, $\eta_T = \frac{372.9W}{565.9W} = 0.659$ transfer efficiency was calculated.

As mentioned in Sect. 3.20, $\eta_U(\lambda) = 0.59$ upper state efficiency was also assumed [11].

Since both which $\eta_T(\lambda)$ and $\eta_U(\lambda)$ remain nearly constant within each of the five absorption bands, we then reach simplified equation for one Sun pump rate.

$$W_p' = \eta_T \eta_U \frac{4}{N_t D} \int \frac{I(\lambda)}{h\upsilon(\lambda)} \{1 - exp[-\alpha(\lambda)L]\} d\lambda$$

$$= \eta_T \eta_U \frac{4}{N_t D} \sum_1^5 F_i \tag{3.146}$$

$$= 0.659 \times 0.59 \times \frac{4}{1.38 \times 10^{20} \text{ cm}^{-3} \times 0.4} \times 5.345 \times 10^{16} \frac{1}{\text{cm}^2\text{s}}$$

$$= 1.506 \times 10^{-3} \frac{1}{\text{s}} \tag{3.165}$$

Calculation of threshold pump rate W_{pth}

For the 2.5 cm length Nd:YAG laser rod

$$\sigma = 2.8 \times 10^{-19} \text{ cm}^2, \ N_t = 1.38 \times 10^{20} \text{ cm}^{-3} \quad R_1 = 0.998 \quad R_2 = 0.98$$

$$\gamma = \alpha + \frac{1}{2}\left[ln\left(\frac{1}{R_1}\right) + ln\left(\frac{1}{R_2}\right)\right]$$

$$= 0.002 \text{ cm}^{-1} \times 2.5 \text{ cm} + \frac{1}{2}(0.002 + 0.0202) = 1.61\% \tag{3.166}$$

$$W_{pth} = \frac{\gamma}{\sigma \tau_e N_t l} = \frac{0.0161}{2.8 \times 10^{19} \text{ cm}^2 \times 230 \times 10^{-6} \text{ s} \times 1.38 \times 10^{20} \text{ cm}^{-3} \times 2.5 \text{ cm}}$$

$$= 0.725 \text{ s}^{-1} \tag{3.167}$$

Calculation of solar laser output power

$$P_{out} = Ah\upsilon\left(\frac{N_t l}{\gamma}\right) \frac{1}{2} ln \frac{1}{R_2}\left[CW_p' - \frac{\gamma}{\sigma \tau_e N_t l}\right] = \eta_s'\left(CW_p' - W_{pth}\right)$$

$$= 0.1256 \text{ cm}^2 \times 6.63 \times 10^{-34} \text{ J S} \times 2.82 \times 10^{14} \text{ S}^{-1}$$

$$\times \left(\frac{1.38 \times 10^{20} \text{ cm}^{-3} \times 2.5 \text{ cm}}{0.0161}\right) \frac{1}{2} ln \frac{1}{0.98}$$

$$\times \left(2301.3 \times 1.506 \times 10^{-3}\frac{1}{\text{s}} - 0.725\frac{1}{\text{s}}\right)$$

$$= 5.085 \text{ J}\left(3.468\frac{1}{\text{s}} - 0.725\frac{1}{\text{s}}\right) = 13.94 \text{ W} \tag{3.168}$$

Calculation of $\frac{P_{in}}{P_{pth}}$ ratio

$$x = \frac{P_{in}}{P_{pth}} = \frac{W_p}{W_{pth}} = \frac{CW'_p}{W_{pth}} = \frac{3.468\frac{1}{s}}{0.725\frac{1}{s}} = 4.784$$

Calculation of threshold pump power P_{pth}

$$P_{pth} = \frac{P_{in}}{x} = \frac{565.9\ W}{4.784} = 118.3\ W$$

Calculation of solar to laser power conversion efficiency η

With 0.636 m^2 collection area, at 890 W/m^2 solar irradiance, 565.9 W incoming solar power was calculated.

$$\eta = \frac{P_{out}}{P_{in}} = \frac{13.94\ W}{565.9\ W} = 2.46\%$$

Calculation of solar laser slope efficiency η_{slope}

$$\eta_{slope} = \frac{P_{out}}{(P_{in} - P_{th})} = \frac{P_{out}}{P_{in}\left(1 - \frac{P_{th}}{P_{in}}\right)} = \eta\frac{1}{\left(1 - \frac{1}{x}\right)}$$

$$= \eta\frac{x}{x-1} = 2.46\%\frac{4.784}{4.784 - 1} = 3.11\%$$

3.28.2 Classical Analytical Method of the End-Side-Pumped Laser

The following equations are commonly used classical analytical method for calculating laser output power P_{out}, slope efficiency η_s and threshold pump power P_{th} of solid-state lasers [2].

$$P_{out} = \frac{1-R}{1+R}\left(\frac{2\eta_{OVP}\eta_T\eta_A\eta_U\eta_B}{\delta - lnR}P_{in} - AI_s\right) \qquad (3.158)$$

$$\eta_s = \frac{1-R}{1+R}\left(\frac{2\eta_{OVP}\eta_T\eta_A\eta_U\eta_B}{\delta - lnR}\right) \qquad (3.159)$$

$$P_{th} = \frac{\delta - lnR}{2\eta_{OVP}\eta_T\eta_A\eta_U\eta_B}AI_s \qquad (3.160)$$

where $I_s = \frac{h\upsilon}{\tau\sigma} = \frac{6.63\times10^{-34}\ JS\times2.82\times10^{14}\ s^{-1}}{230\times10^{-6}\ S\times2.8\times10^{-19}\ cm^2} = 2.90\ \frac{kW}{m^2}$.

For the side-pumped solar laser in Fig. 3.23, all other important parameters and laser output power are calculated by (3.158), (3.159) and (3.160) and listed by Table 3.5.

Table 3.5 Design parameters and output performance of the end-side-pumped solar laser

Parameters	
Irradiance (W/m^2)	890
Collection area (m^2)	0.636
P_{IN} (W)	565.9
Rod diameter (mm)	4
Length l (mm)	25
A (cm^2)	0.1256
I_S (kW/cm^2)	2.90
AI_S (W)	364.2
α (cm^{-1})	0.002
$2\,\alpha\,l$	0.01
δ_M	0.004
δ_D	0.000
$\delta = 2\alpha l + \delta_M + \delta_D$	0.014
R	0.98
(1-R)/(1 + R)	0.0101
δ - lnR	0.0342
η_{OVP}	0.16
P_{SOURCE} (Zemax) (W)	90.545
$P_{TRANSFER}$ (Zemax) (W)	59.65
η_T	0.659
$P_{ABSORBED}$ (Zemax) (W)	49.05
η_A	0.822
η_U	0.59
η_B	1.00
$\eta = \eta_{OVP}\eta_T\eta_A\eta_U\eta_B$	0.0511
Analytical Calculation	
P_{OUT} (W)	13.41
Total η_{SLOPE} (%)	3.02
P_{TH} (W)	121.9
Solar-to-laser conversion efficiency (%)	2.37

3.28.3 LASCAD™ Numerical Analysis
of the End-Side-Pumped Solar Laser

The absorbed pump flux data from the Zemax® analysis of the end-side-pumped solar laser in Fig. 3.34 was processed by LASCAD™ software to evaluate its solar laser output performances. The stimulated emission cross-section of 2.8×10^{-19} cm^2, the fluorescence life time of 230 μs and an absorption and scattering loss of 0.002 cm^{-1} for the Nd:YAG medium were adopted in LASCAD™ analysis. The mean absorbed and intensity-weighted solar pump wavelength of 660 nm [14] was also used in the analysis. For the 25 mm diameter, 1.0 at.% Nd:YAG rod with length $L_R = 25$ mm, the amount of absorption and scattering losses was 2 α $L_R = 1.0\%$. Assuming 0.4% of imperfect HR and AR coating losses, the round-trip loss was increased to 1.4%. The diffraction losses depend heavily on rod diameter, resonator length and RoC of the resonator mirrors. LASCAD™ beam propagation method (BPM) resulted in a negligible diffraction loss when HR1064 nm end mirror and PR1064 nm output mirror, all with RoC $= \infty$, were placed very close to the laser rod. Final round-trip loss of 1.4% was calculated. Consequently, 13.96 W multimode solar laser power was numerically obtained, as shown by Fig. 3.38.

By considering the incoming solar power of 565.9 W and for the maximum solar laser output power of 13.96 W, solar-to-laser conversion efficiency of 2.47% was calculated for the closely coupled resonant cavity. Effective threshold solar pump power of 9.7 W and maximum effective solar power of 48.3 W was calculated, corresponding to 113.7 W threshold solar power and 565.9 W maximum incoming solar power, respectively. Solar laser slope efficiency of 3.09% was hence calculated. Maximum pump power/ threshold pump power ratio of 4.98 was calculated. All the above mentioned parameters are indicated in Table 3.6.
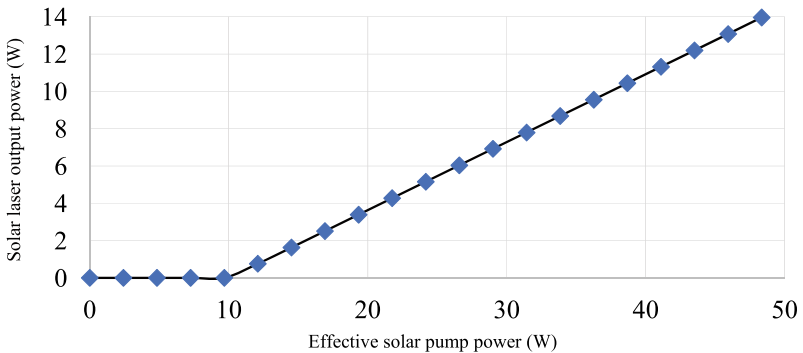
| Effective solar pump power | 9.7 W | 48.3 W |
| Incoming solar power | 113.7 W | 565.9 W |

Fig. 3.38 Numerically calculated solar laser output power versus effective incoming solar power (Detector pixies 40 × 40 × 25) for 1 mm laser cavity length

Table 3.6 Solar laser output performance by different analysis methods

	Laser output power (W)	Threshold pump power (W)	Solar-to-laser conversion efficiency (%)	Laser slope efficiency (%)	Maximum pump power/threshold pump power ratio
Modified analysis	13.94	118.4	2.46	3.11	4.78
Classical analysis	13.41	121.9	2.37	3.02	4.64
LASCAD$_{Max}$	13.96	113.7	2.47	3.09	4.98
LASCAD$_{120\,mm}$	12.26	106.8	2.17	2.67	5.30
Experimental	12.30	125.8	2.17	2.79	4.50

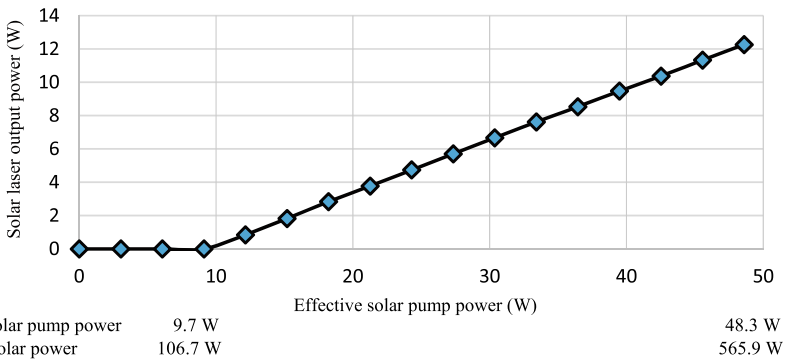|		
Effective solar pump power	9.7 W	48.3 W
Incoming solar power	106.7 W	565.9 W

Fig. 3.39 Numerically calculated solar laser output power versus effective incoming solar power (Detector pixies 40 × 40 × 25) for 120 mm cavity length

Similarly, for the laser resonator with $L = 120$ mm length, as shown in Fig. 3.39 and under the same pumping condition, 12.26 W laser output power, 106.8 W threshold pump power, 2.17% solar-to-laser conversion efficiency, 2.67% laser slope efficiency and 5.30 maximum pump power/threshold pump power ratio were calculated by LASCAD$^©$ software, as shown in Table 3.6. (See Chaps. 2 and 5 for Zemax$^®$ and LASCAD$^{™}$ laser power calculation methods for the solar laser with definite resonant cavity).

3.28.4   Comparison of Different Analyses for the End-Side-Pumped Solar Laser

Discussions

As shown by Table 3.6, both the modified and the LASCAD$_{Max}$ analyses predicted nearly the same amount of maximum extractable multimode laser power and solar-to-laser conversion efficiency when a PR1064 nm output mirror was closely placed near

the Nd:YAG laser rod. This happened when $\eta_B = 1$ overlap efficiency was assumed in the modified analysis. Classical analysis offered a slightly reduced accuracy in laser output power and efficiency predictions, as shown by Table 3.6.

It is important to point out that both the modified and the classical analyses were not effective in predicting the output power from a laser resonant cavity with a certain cavity length L ($\eta_B < 1$), since it was very difficult to calculate analytically the beam overlap efficiency of solar pumped solid-state lasers, as mentioned in Sect. 3.22.

Zemax® and LASCAD™ analyses, however, were effective in the laser output power prediction of a solar laser with certain cavity length. Detailed analysis method will be provided in Sect. 6.2.1 of Chap. 6.

When the PR1064 nm output mirror was positioned 120 mm away from the rod, there was a noticeable reduction in beam overlap efficiency ($\eta_B < 1$), consequently, 12.26 W solar laser power was numerically calculated by Zemax® and LASCAD$_{120\,mm}$ analyses, as shown by Fig. 3.39 and confirmed by experimental result [14]. As for the prediction of threshold solar pump power, all the analyses failed to a considerable extent, leading normally to a much smaller threshold power prediction, as compared to the experimental value in Table 3.6.

Homework with Solution 1

Calculation of Resonant Modes Numbers within a Cavity

Solution

For a single plane wave: $\vec{E}\left(\vec{r}, t\right) = \vec{E}_0 e^{i2\pi v t - i\vec{k}\cdot\vec{r}}$.

Where $\vec{E}_0$ is field amplitude, v is light wave frequency, $\vec{r}$ is space coordinate vector and $\vec{k}$ is light wave vector. In free space, $\vec{k}$ can be any value. However, in hollow cavity, "v" are with bounding limitations, only discrete values can exist. We consider stationary waves within a cubic hollow cavity (Fig. 3.40).
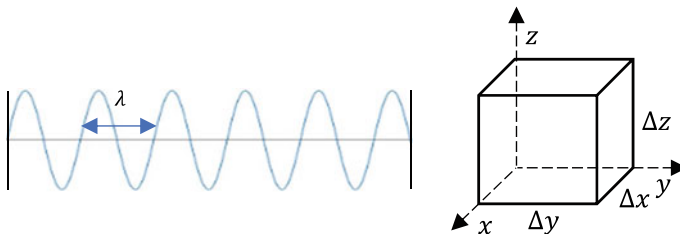

Fig. 3.40 Schematics of a stationary wave and a cubic hollow cavity with Δx, Δy, Δz dimension

We therefore obtain

$$\Delta x = m\frac{\lambda}{2} \quad \Delta y = n\frac{\lambda}{2} \quad \Delta z = q\frac{\lambda}{2} \tag{3.169}$$

where: m, n, q can be any integers

For $k = \frac{2\pi}{\lambda}$ the three components of k should meet the following conditions (Fig. 3.41)

$$k_x = \frac{\pi}{\Delta x}m, \quad k_y = \frac{\pi}{\Delta y}n, \quad k_z = \frac{\pi}{\Delta z}q \tag{3.170}$$

The interval between modes can hence be calculated

$$\Delta k_x = \frac{\pi}{\Delta x}, \quad \Delta k_y = \frac{\pi}{\Delta y}, \quad \Delta k_z = \frac{\pi}{\Delta z} \tag{3.171}$$

Each mode occupies a unit volume element in "k" space (Fig. 3.42)

$$\Delta k_x \Delta k_y \Delta k_z = \frac{\pi^3}{\Delta x \Delta y \Delta z} = \frac{\pi^3}{V} \tag{3.172}$$

In $\vec{k}$ space, the volume between $\left|\vec{k}\right|$ and $\left|\vec{k}\right| + d\left|\vec{k}\right|$ is:

$$\frac{1}{8}4\pi \left|\vec{k}\right|^2 d\left|\vec{k}\right| \tag{3.173}$$

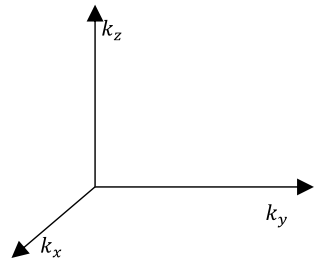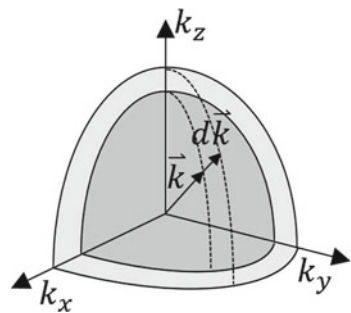**Fig. 3.41** Presentation of k-space in k_x, k_y, k_z components

Fig. 3.42 $\vec{k}$ space presentation for calculating the volume between $\vec{k}$ and $\vec{k} + d\left|\vec{k}\right|$

Therefore, the number of modes within $\left\lfloor \vec{k} \right\rfloor$ and $\left\lfloor \vec{k} \right\rfloor + d\left\lfloor \vec{k} \right\rfloor$

$$\frac{\frac{1}{8}4\pi \left\lfloor \vec{k} \right\rfloor^2 d\left\lfloor \vec{k} \right\rfloor}{Unit\ volume\ of\ k\ space} = \frac{\frac{1}{8}4\pi \left\lfloor \vec{k} \right\rfloor^2 d\left\lfloor \vec{k} \right\rfloor}{\frac{\pi^3}{V}} = \frac{1}{8}4\pi \left\lfloor \vec{k} \right\rfloor^2 d\left\lfloor \vec{k} \right\rfloor \frac{V}{\pi^3} \tag{3.174}$$

Since

$$\left\lfloor \vec{k} \right\rfloor = \frac{2\pi}{\lambda} = \frac{2\pi}{\frac{c}{\upsilon}} = \frac{2\pi \upsilon}{c} \tag{3.175}$$

$$d\left\lfloor \vec{k} \right\rfloor = \frac{2\pi}{c} d\upsilon \tag{3.176}$$

Also since there are two modes (spin angular momentum of $(\pm \hbar)$) possible for each value of k, the total number of modes within $\upsilon \leftrightarrow \upsilon + d\upsilon$

$$2 \times \frac{1}{8}4\pi \left(\frac{2\pi \upsilon}{c}\right)^2 \frac{2\pi}{c} d\upsilon \frac{V}{\pi^3} = \frac{8\pi \upsilon^2}{c^3} V d\upsilon \tag{3.177}$$

where V is the volume of the cavity. $\rho(\nu)$ is defined as the number of modes per unit volume and per unit frequency range, the number of mode per unit volume per unit frequency is therefore calculated.

$$Number\ of\ modes = \frac{8\pi \upsilon^2}{c^3} \tag{3.178}$$

Homework with Solution 2

Deriving Solar Spectral Irradiance from Planck's Law

In experimental work, solar irradiance distribution as a function of wavelength is preferred and the radiation law take the form

$$I(\lambda, T) = \frac{2hc^2}{\lambda^5} \frac{1}{e^{\frac{hc}{\lambda kT}} - 1} \tag{3.22}$$

Please deduce solar spectral irradiance (3.22) from Planck's law (3.21)

$$\rho(\upsilon, T) = \frac{8\pi h \upsilon^3}{c^3} \frac{1}{e^{\frac{h\upsilon}{kT}} - 1} \tag{3.21}$$

Solution

By considering energy inavariance in wavelength and frequency domains

$$\rho(\lambda, T)d\lambda = -\rho(\upsilon, T)d\upsilon \tag{3.179}$$

then

$$\rho(\lambda, T) = -\rho(\upsilon, T)\frac{d\upsilon}{d\lambda} \tag{3.180}$$

Since

$$\upsilon = \frac{c}{\lambda}, \; \frac{d\upsilon}{d\lambda} = -\frac{c}{\lambda^2} \tag{3.181}$$

then

$$\rho(\lambda, T) = \rho(\upsilon, T)\frac{c}{\lambda^2} \tag{3.182}$$

Since full solid angle equals 4π,
Planck's formula per Steradian is therefore obtained by dividing (3.21) by 4π.

$$\rho(\upsilon, T) = \frac{2h\upsilon^3}{c^3}\frac{1}{e^{\frac{h\upsilon}{kT}} - 1} \tag{3.21}$$

Consequently, $\rho(\lambda, T)$ can be deduced from $\rho(\upsilon, T)$

$$\rho(\lambda, T) = \rho(\upsilon, T)\frac{c}{\lambda^2} = \frac{2h\upsilon^3}{c^3}\frac{1}{e^{\frac{h\upsilon}{kT}} - 1}\frac{c}{\lambda^2} = \frac{2hc}{\lambda^5}\frac{1}{e^{\frac{hc}{\lambda kT}} - 1} \tag{3.183}$$

Solar spectral irradiance $I(\lambda)$ can be obtained by multiplying (3.183) by c

$$I(\lambda, T) = \rho(\lambda)c \tag{3.23}$$

Consequently, we obtain solar spectral irradiance as a function of wavelength λ (as well as temperature T)

$$I(\lambda, T) = \frac{2hc^2}{\lambda^5}\frac{1}{e^{\frac{hc}{\lambda kT}} - 1} \tag{3.22}$$

Homework with Solution 3

Deriving Stefan-Boltzmann's Law from Planck's Law

Please deduce Stefan-Boltzmann's law (3.25)

$$I = \frac{P}{A} = \sigma T^4 = \frac{2\pi^5}{15} \frac{k^4}{c^2 h^3} T^4 = 5.67 \times 10^{-8} \times T^4 \left[\frac{\text{W}}{\text{m}^2} \right] \qquad (3.25)$$

from Plank's formula (3.21)

$$\rho(\upsilon) = \frac{8\pi h \upsilon^3}{c^3} \frac{1}{e^{\frac{h\upsilon}{kT}} - 1} \qquad (3.21)$$

Solution

Plank's formula in terms of photon irradiance

$$I(\upsilon) = \rho(\upsilon)c = \frac{8\pi h \upsilon^3}{c^2} \frac{1}{e^{\frac{h\upsilon}{kT}} - 1} \qquad (3.184)$$

Total photon irradiance I over the whole frequency spectrum

$$I = \frac{P}{A} = \int_0^\infty I(\upsilon)d\upsilon = \int_0^\infty \frac{8\pi h \upsilon^3}{c^2} \frac{1}{e^{\frac{h\upsilon}{kT}} - 1} d\upsilon = \frac{8\pi h}{c^2} \int_0^\infty \frac{\upsilon^3}{e^{\frac{h\upsilon}{kT}} - 1} d\upsilon \quad (3.185)$$

If we assume

$$x = \frac{h\upsilon}{kT} \quad \text{then} \quad \upsilon = \frac{kT}{h}x, \ d\upsilon = \frac{kT}{h}dx \qquad (3.186)$$

For 4π solid angle

$$
\begin{aligned}
I = \frac{P}{A} &= \frac{8\pi h}{c^2} \int_0^\infty \frac{\left(\frac{kT}{h}x\right)^3}{e^x - 1} \frac{kT}{h} dx = \frac{8\pi k^4 T^4}{c^2 h^3} \int_0^\infty \frac{x^3}{e^x - 1} dx \\
&= \frac{8\pi k^4 T^4}{c^2 h^3} \frac{\pi^4}{15} = \frac{8\pi^5}{15} \frac{k^4}{c^2 h^3} T^4 \\
&= \sigma' T^4 \qquad\qquad\qquad\qquad\qquad\qquad\qquad\qquad\qquad (3.187)
\end{aligned}
$$

Since

$$h = 6.63 \times 10^{-34} \text{ J} \cdot \text{s} \quad k = 1.38 \times 10^{-23} \frac{\text{J}}{\text{K}}$$

Radiation constant $\sigma = \frac{1}{4}\sigma'$ of Stefan-Boltzmann's law can be calculated

$$I = \frac{P}{A} = \sigma T^4 = \frac{2\pi^5}{15}\frac{k^4}{c^2 h^3}T^4 = 5.67 \times 10^{-8} \times T^4 \qquad (3.25)$$

according to 2019 redifinition of SI base units

$$I = \frac{2\pi^5}{15}\frac{k^4}{c^2 h^3}T^4 \quad \text{Dimensional analysis}: \quad \left[\frac{W}{m^2}\right] = \left[\frac{J}{m^2 \cdot s}\right] = \left[\frac{\frac{J^4}{K^4} \cdot K^4}{\frac{m^2}{s^2} \cdot J^3 \cdot s^3}\right] \qquad (3.188)$$

Homework with Solution 4

Deriving Wien's Displacement Law from Planck's Law

Please deduce Wien's displacement law (3.27)

$$\lambda_{max}T = 2.898\,\mu m \cdot K \qquad (3.27)$$

from Planck's law (3.22)

$$\rho(\lambda) = \frac{8\pi hc}{\lambda^5}\frac{1}{e^{\frac{hc}{\lambda kT}} - 1} \qquad (3.22)$$

Solution

By taking derivative of $\rho(\lambda)$ with respect to λ:

$$\frac{d\rho(\lambda)}{d\lambda} = \frac{d}{d\lambda}\left(\frac{8\pi hc}{\lambda^5}\frac{1}{e^{\frac{hc}{\lambda kT}} - 1}\right) \qquad (3.189)$$

$$\frac{d\rho(\lambda)}{d\lambda} = \frac{8\pi hc}{e^{\frac{hc}{\lambda kT}} - 1}\frac{d}{d\lambda}(\lambda^{-5}) + \frac{8\pi hc}{\lambda^5}\frac{d}{d\lambda}\left(\frac{1}{e^{\frac{hc}{\lambda kT}} - 1}\right)$$

$$= \frac{8\pi hc}{e^{\frac{hc}{\lambda kT}} - 1}\frac{-5}{\lambda^6} + \frac{8\pi hc}{\lambda^5}\frac{-1}{\left(e^{\frac{hc}{\lambda kT}} - 1\right)^2}e^{\frac{hc}{\lambda kT}}\frac{d\left(\frac{hc}{\lambda kT}\right)}{d\lambda} \qquad (3.190)$$

Peak $\rho(\lambda)$ can be found by applying

$$\frac{d\rho(\lambda)}{d\lambda} = 0 \qquad (3.191)$$

Then

$$\frac{d\rho(\lambda)}{d\lambda} = \frac{-8\pi hc}{e^{\frac{hc}{\lambda kT}} - 1} \frac{5}{\lambda^6} + \frac{-8\pi hc}{\lambda^5} \frac{e^{\frac{hc}{\lambda kT}}}{\left(e^{\frac{hc}{\lambda kT}} - 1\right)^2} \left(-\frac{hc}{kT}\frac{1}{\lambda^2}\right) = 0 \qquad (3.192)$$

$$\frac{8\pi hc}{e^{\frac{hc}{\lambda kT}} - 1} \frac{5}{\lambda^6} = \frac{8\pi hc}{\lambda^7 kT} hc \frac{e^{\frac{hc}{\lambda k}}}{\left(e^{\frac{hc}{\lambda kT}} - 1\right)^2} \qquad (3.193)$$

Finally

$$5 = \frac{hc}{\lambda kT} \frac{e^{\frac{hc}{\lambda kT}}}{e^{\frac{hc}{\lambda kT}} - 1} \qquad (3.194)$$

If we assume

$$\frac{hc}{\lambda kT} = x \qquad (3.195)$$

Then:

$$5 = x\frac{e^x}{e^x - 1}, \quad xe^x = 5\left(e^x - 1\right) \qquad (3.196)$$

where $x = 4.965$ equalize both side of the above equation.
Consequently

$$\frac{hc}{\lambda kT} = 4.965 \qquad (3.197)$$

Which happens when $\lambda = \lambda_{\max}$

$$\lambda_{\max} T = \frac{hc}{4.965 \text{ k}} = \frac{6.63 \times 10^{-34} \times 3 \times 10^8}{4.965 \times 1.38 \times 10^{-23}} \qquad (3.198)$$

Wien's displacement law is finally deduced

$$\lambda_{\max} T = 2.898 \text{ } \mu\text{m } K \qquad (3.27)$$

References

1. Svelto, O.: Principles of Lasers, 5th edn. Springer, New York, NY (2016). https://books.goo
   gle.pt/books/about/Principles_of_Lasers.html?id=ioywRI5W2HEC&redir_esc=y
2. Koechner, W.: Solid-State Laser Engineering, 6th edn. Springer, Berlin Heidelberg (2006).
   https://link.springer.com/book/10.1007/978-3-662-14219-6

3. Yariv, A., Gordon, J. P.: The Laser*. Proceedings of the IEEE (1963). https://www.mindat.org/reference.php?id=12781943

4. Renk, K. F.: Basics of Laser Physics, 2nd edn. Springer Science & Business Media (2012). https://books.google.pt/books/about/Basics_of_Laser_Physics.html?id=dpVDTLPySTQC&redir_esc=y

5. Haken, H.: Laser Theory. Springer, Berlin Heidelberg (1984). https://books.google.pt/books/about/Laser_Theory.html?id=wzLtCAAAQBAJ&redir_esc=y

6. Siegman, A.E.: Lasers. University Science Books, Mill Valley, CA (1986). https://books.google.pt/books/about/Lasers.html?id=1BZVwUZLTkAC&redir_esc=y

7. Dickson, L.: Characteristics of a propagating gaussian beam. Appl. Opt. **9**, 1854–1861 (1970). https://opg.optica.org/ao/abstract.cfm?uri=ao-9-8-1854

8. Stoehr, H., Mensing, F., Helmcke, J., Sterr, U.: Diode laser with 1 Hz linewidth. Opt. Lett. **31**, 736–738 (2006). https://opg.optica.org/ol/abstract.cfm?uri=ol-31-6-736

9. Mandel, L.: Photon degeneracy in light from optical maser and other sources*. J. Opt. Soc. Am. **51**, 797–798 (1961). https://opg.optica.org/josa/abstract.cfm?uri=josa-51-7-797

10. Hwang, I. H., Lee, J. H.: Efficiency and threshold pump intensity of CW solar-pumped solid-state lasers. IEEE J. Quantum Electron. **27**(9), 2129–2134 (1991). https://ieeexplore.ieee.org/document/135171

11. Laporta, P., Magni, V., Svelto, O.: Comparative study of the optical pumping efficiency in solid-state lasers. IEEE J. Quantum Electron. **21**(8), 1211–1218 (1985). https://ieeexplore.ieee.org/document/1072800

12. Barnes, N. P. Solid state laser from an efficiency perspective. IEEE J. Sel. Top. Quantum Electron. (June 2007). https://ieeexplore.ieee.org/document/4244407

13. Liang, D., Vistas, C. R., Garcia, D., Tibúrcio, B. D., Catela, M., Costa, H., Guillot, E., Almeida, J.: Most efficient simultaneous solar laser emissions from three Ce:Nd:YAG rods within a single pump cavity. Sol. Energy Mater. Sol. Cells. **246**, 111921 (2022). https://www.sciencedirect.com/science/article/abs/pii/S0927024822003403#!

14. Liang, D., Almeida, J.: Highly efficient solar-pumped Nd:YAG laser. Opt. Express **19**, 26399–26405 (2011). https://opg.optica.org/oe/fulltext.cfm?uri=oe-19-27-26399&id=225792

15. Weksler, M., Shwartz, J.: Solar-pumped solid-state lasers. IEEE J. Quantum Electron. **24**(6), 1222–1228 (1988). https://ieeexplore.ieee.org/document/247

16. Lando, M., Kagan, J., Linyekin, B., Dobrusin, V.: A solar-pumped Nd:YAG laser in the high collection efficiency regime. Opt. Commun. **222**, 1 (2003). https://www.sciencedirect.com/science/article/abs/pii/S0030401803016018